Evaluating the Potential of ICESat/GLAS data to Estimate Canopy Height in the New Forest National Park, UK

Irfan Akhtar Iqbal
March, 2010

Course Title:	Geo-Information Science and Earth Observation for Environmental Modelling and Management
Level:	Master of Science (M.Sc.)
Course Duration:	September 2008 - March 2010
Consortium partners:	University of Southampton (UK) Lund University (Sweden) University of Warsaw (Poland) International Institute for Geo-Information Science and Earth Observation (ITC) (The Netherlands)
GEM thesis number:	2010-14

Evaluating the Potential of ICESat/GLAS data to Estimate Canopy Height in the New Forest National Park, UK

by

Irfan Akhtar Iqbal

Thesis submitted to the International Institute for Geo-information Science and Earth Observation in partial fulfilment of the requirements for the degree of Master of Science in Geo-information Science and Earth Observation for Environmental Modelling and Management

Thesis Assessment Board

Chair	Prof. Dr. Ing. Wouter Verhoef
External Examiner	Prof. Dr. hab. Katarzyna Dąbrowska-Zielińska
	Prof T.P. Dawson
1st Supervisor	Dr. Jadunandan Dash (University of Southampton, UK)
2nd Supervisor	Drs. Raymond Nijmeijer (ITC, the Netherlands)
Course coordinator	M. Sc. Andre Kooiman

ITC
UNIVERSITY OF TWENTE.
FACULTY OF GEO-INFORMATION SCIENCE AND EARTH OBSERVATION

"If we knew what it was we were doing, it would not be called research, would it?"

Albert Einstein (1879-1955)

Abstract

Geoscience Laser Altimeter System (GLAS) aboard Ice, Cloud and land Elevation Satellite (ICESat) is a new generation of spaceborne LiDAR which was launched in January, 2003. It is the first spaceborne instrument which can digitize the backscattered waveform and offer global coverage. Among others, scientific objectives of the mission include precise measurement of land topography and vegetation canopy heights. GLAS waveforms are affected by within-footprint topographic variations. This leads to uncertainty in accurate ground detection from the waveform which, in turn, is reflected in canopy heights. Existing approach of waveform processing suggests Gaussian decomposition of the waveform to a maximum of six modes. Peak of the last, out of six, mode is considered to be representing the ground return. Six modes, however, are not always sufficient to fit the waveform, resulting in discrepant information. This emphasizes the need of efficient waveform processing for accurate estimation of vegetation height.

This study investigated GLAS elevation products, insights from which were inputs in canopy heights estimation from 'raw' waveforms. Further, canopy height estimates from GLAS were compared with those of airborne LiDAR heights acquired under similar environmental and topographic conditions.

Digital elevation models were created from GLAS point elevations and compared with Ordnance Survey elevations. Possible reasons of uncertainties were analysed, on the basis of which a new method of waveform processing was developed. An automated method, applying Fourier Transformation technique, was used for the efficient detection of ground peak from 'raw' waveform.

Canopy heights retrieved from GLAS waveforms were validated with field measured heights. The new method was able to explain 79% of variation in canopy heights with an RMSE of 3.18 meters, in the study area. In the premises of the study area, a non-coincident airborne LiDAR explained 80% of variation in canopy heights with an RMSE of 2.76 meters.

The unexplained variation in canopy heights retrieved from GLAS data can be due to the possible sources errors; such as, footprint eccentricity, decay of energy between emitted and received energy, clinometric measurements in the field and limited number of sampled footprints.

Results achieved with the new method were encouraging and demonstrated the potential of full-waveform large footprint spaceborne LiDAR in estimating canopy height.

Keywords: GLAS/ICESat, Canopy height, Waveform processing, Full waveform, LiDAR

Acknowledgements

I would like to thank the Beneficent and the Merciful for bestowing on me all the joys of life. Also for helping me win the race against the clock when I was enmeshed in deadlines.

I owe my deepest gratitude to my first supervisor Dr. Jadunandan Dash for his inspiring interest and continual guidance. From scratch until yet, it was only possible with your encouragement and facilitation. Throughout the course of this work, it was an intensive learning experience. The pleasure, of working under your 'active' supervision especially during my stay at Southampton, is all mine.

My second supervisor, Dr. Raymond Nijmeijer, deserves a vote of thanks for shaping this work. Your critical comments along with friendly attitude are highly commended.

It is a pleasure to thank the GEM Consortium Board for providing me an opportunity to arrive at this work. Also, I would like to show my heartfelt gratitude to the lecturers and management personnel in University of Southampton, UK; Lund University, Sweden; University of Warsaw, Poland; and ITC, the Netherlands. Without your cooperation, the course would not have been a smooth sail.

I wish to express my sincere thanks to David Korn, Associate Scientist NSIDC; Jane Smith, Planning Manager Forestry Commission; and Charlotte Phillips, Research Project Coordinator, Ordnance Survey for addressing my queries.

My sincere thanks are due to Matthew Sumnall (University of Southampton) for sharing his work and time with me. I hope we remain in the loop.

I feel compelled to single out Shola, who remained the main source of inspiration behind this work. Thank you for sharing my frustrations and excitements all the way long. Stay well.

During this course I have collaborated with many colleagues, the 'GEM Family', for whom I have great regard. My life would not have been better without you. On practical level, I thank Vincent Odongo for his company during our stay in Southampton. You really know the way I usually thank you.

I warmly thank Raja Ghayyas Ahmad, Assistant Professor of Forestry PFI, who had made his support available in many ways over a decade.

I cannot forget to extend my loving thanks to my family and friends back home, who have a formative influence on me over the years.

Table of contents

List of figures

List of tables

1. Introduction

1.1. Background

Global concerns like climate change, global warming and greenhouse effect can undoubtedly be assigned to anthropogenic activities modifying Earth's atmosphere at a global scale (Malhi and Grace, 2000). Crucial in this context are the emissions from various carbon sources, as well as sinks when they are disturbed, which underscores the importance of vigilance to global carbon budget. The United Nations Framework Convention on Climate Change (UNFCCC, 1997) came up with the realization to reduce carbon emissions and greenhouse gases concentration to prevent unsafe anthropogenic interference with the climate. Linked to this was the Kyoto Protocol, obliging the member countries to reduce their carbon emissions utilizing their forest ecosystems (UNFCCC, 1997). Recently, the Copenhagen Summit (December 2009) also recognized the crucial role of forests in reducing emission of green house gases (UNFCCC, 2009a), as the forest ecosystems are significant pools of global carbon. By estimating the structural attributes (e.g. aboveground biomass) of these ecosystems, the amount of carbon sequestered can be calculated as half the dry weight of biomass (Drake et al., 2002, Houghton, 2008, UNFCCC, 2009b, IPCC, 2003). This highlights the importance of precise knowledge on the carbon capacity of these ecosystems for addressing the issue of global warming. In general, aboveground biomass (AGB) is estimated by using the diameter of a tree at breast height (DBH) (Keller et al., 2001). Though straightforward, direct estimation of biomass (through DBH) on ground is time consuming as well as expensive (Houghton, 2005) and sometimes involves destructive sampling (Hiratsuka et al., 2003).

On the other hand, due to its aesthetics of spatial and temporal coverage, Remote Sensing has an edge over conventional field measurement methods. Remote Sensing techniques commit to save time and money in estimating biomass. Its performance is limited by fact that DBH cannot be directly measured from it. However, other biophysical parameters like canopy height and canopy cover can serve as a proxy for estimating the amount of AGB. Several studies have attempted to use remotely sensed data (passive optical as well as active microwave (RADAR)) for estimating the biophysical parameters of vegetation and in turn, to estimate AGB e.g. (Dobson et al., 1992, Kaufman et al., 1990, Muukkonen and Heiskanen, 2007). However, the accuracy and sensitivity of these two data types drops-off in areas of closed canopies and high-biomass (Waring et al., 1995). RADAR is reported to achieve a desired accuracy level only in structurally homogeneous vegetation with relatively low biomass (Boudreau et al., 2008). Also, data derived from optical (passive) sensors are confined to two dimensions (x, y) only, and the vertical diversity (z-component) of vegetation is oversighted. Lack of ample information on the vertical component

results in complexities, when one is interested in canopy height estimation for quantifying AGB.

On the contrary, Light Detection and Ranging (LiDAR) directly measures the vertical component of vegetation, thus has the potential to measure the structural attributes of vegetation (Lefsky et al., 2002b, Dubayah et al., 2000). Though the working principle of LiDAR is the same as RADAR, the former operates in shorter wavelength and has less beam divergence (Gerck and Hurtak, 1992). These qualities enable LiDARs to capture local variation and conduct regionally focussed studies on reliable and short-term basis. Moreover, for ecosystem management, tree heights and vegetation density derived from LASER altimetry prove to be important inputs for modelling processes in the biosphere.

1.2. LiDARs and LASER Altimetry

Light **A**mplification by **S**timulated **E**mission of **R**adiation (LASER) is a device that emits electromagnetic radiations through simulated emission in which light of narrow wavelength channels is emitted. These laser pulses are used to detect and determine range of object through a technology known as **Li**ght **D**etection **a**nd **R**anging (LiDAR). LASERs are active sensors, since they emit their own radiations. When used to workout the height of targets, it is termed as LiDAR or LASER altimetry (Dubayah et al., 2000).

A LASER altimeter produces short pulses of LASER light, which are captured by a telescope, after bouncing back when they are intercepted by a target. The time delay between the pulse emission and reception, when it returns, is translated to distance and represents the range of the target. The underlying principle is a simple distance, speed and time relationship, which is given by equation 1.1:

$$S \text{ (distance)} = v \text{ (speed)} \times t \text{ (time)} \qquad (1.1)$$

The speed here is the speed of light (c) and hence always taken as $3x10^8$ m/sec. Since the distance travelled is a round trip distance, half of it is the range of an object or target.

1.2.1. LASER Altimetry and its application

Due to its unique capability to capture elevation information, LASER altimetry has been used for various purposes, such as, Digital Elevation Model (DEM) generation (Ma, 2005), canopy (Næsset, 1997a, Næsset and Bjerknes, 2001) and cloud height (Gondal and Mastromarino, 2000) estimation, and elevation changes in polar ice sheets (Slobbe et al., 2008). Both airborne and spaceborne altimeters are giving promising results, with improved accuracy, as the technology advances. St-Onge et al. (2003) reported the typical absolute vertical accuracy of LiDAR data to be 10-40 cm from an airborne platform and 1000 cm from a spaceborne LiDAR system. However, Suárez et al. (2005) noted that airborne LiDAR is capable of achieving an accuracy of 15-20 cm in vertical and 20-30 cm in horizontal.

In addition to its accuracy, the third dimension (*z*-axis) of LASER altimetry is used for topographic mapping, where it substantially reduces the time and effort as compared to traditional field measurement methods. As LASER altimetry contains the least amount of obscuration and shadowing, it can also be used to generate accurate 3D city models (Ackermann, 1999). Similarly, precise terrain height information can, for example, be used to optimize water distribution and drainage processes, which are of prime importance in precision farming (Geolas, 2007).

Apart from these, in Forestry, one of the applications of LiDARs is canopy height and crown cover estimation as they are of direct interest to the foresters (Suárez et al., 2005) for forest management. Because canopy height has a strong relationship with other biophysical parameters, such as biomass and volume (Lefsky et al., 2002a, Næsset, 1997b, Nilsson, 1996), its accurate estimation is imperative.

Essentially, LASER systems are categorized (Dubayah et al., 2000) on the basis of:

a) Method of recording the return pulse – discrete return or full-waveform systems;
b) Size/area of the illuminated spot – small (few centimeters) or medium to large footprint (tens of meters); and
c) Sampling rate/scanning pattern

In forested environment, small-footprint discrete-return LiDAR will only record portions of the canopy structure (because of smaller sampling area). On the other hand, combination of large-footprint and full-waveform LiDARs will be able to record information of canopy as well as sub-canopy level rather than individual trees (Lim et al., 2003). Figure 1.1 illustrates that full-waveform LiDARs digitizes the return pulse as a complete wave; whereas, discrete return records the return pulse at a maximum of five instances. In Figure 1.1, the transmitted pulse is shown in top left corner.

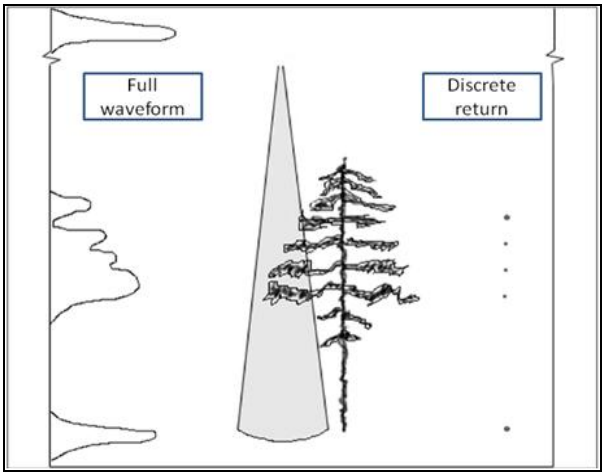

Figure 1.1: Comparison of full-waveform and discrete return LiDARs (adapted from Lim et al. (2003)).

Forestry related, small-footprint airborne laser scanning is well-documented in peer-reviewed literature e.g. Carson et al. (2004) and Lim et al. (2003). However, studies related to estimation of vegetation parameters using large-footprint full-waveform LiDAR are afoot and has a great potential for further exploration, especially in case of **G**eoscience **L**aser **A**ltimeter **S**ystem (GLAS) (see Section 2 for details).

GLAS is a new generation spaceborne LiDAR onboard the **I**ce, **C**loud and land **E**levation **Sat**ellite (ICESat) mission, which was launched on January 13, 2003. GLAS is the first spaceborne instrument which can digitize the backscattered waveform (Wagner et al., 2006). Moreover, it is the first polar-orbiting sensor which combines high precision surface LiDAR with a sensitive dual wavelength cloud and aerosol LiDAR (NASA, 2003) – a characteristic which distinguishes it from other altimeters. Orbiting at about 600 km, GLAS offers global coverage by carrying three lasers (Laser 1, 2 and 3) with only one operational at a time. After the failure of Laser 1, GLAS followed a modified plan of 33 days sub-cycle with a 91 days repeat orbit (Abshire et al., 2005). Under the revised plan, Laser 3 acquired data during February-March, May-June, and October-November (Schutz et al., 2005), until its failure in October, 2008. The latest updates are that Laser 2 has also unexpectedly stopped functioning since October 11, 2009 (NASA, 2009a). However, attempts to restart Laser 2 have recently been initiated, which will be followed for the other two lasers.

Originally, ICESat was launched to monitor polar ice-sheet dynamics and its role in changing the global sea-level (Zwally et al., 2002). However, other scientific objectives of this mission also include surface reflectivity, precise measurement of land topography, ocean surface elevations and vegetation canopy heights. GLAS transmits short pulses (4 ns width equivalent to 60 cm in surface elevation) of infrared (1064 nm) and visible green (532 nm) light at a rate of 40 shots a second

(40 Hz). GLAS documentation assumes that the transmitted pulse is almost a Gaussian and so will be the shape of returned waveform (Brenner et al., 2003). The reflected photons are collected by a telescope of 1 meter diameter and binned at each nanosecond. Each of the 40 shots is telemetered in 544 bins over ice-sheet and land, corresponding to a height of 81.6 m (Brenner et al., 2003). In steeply sloped areas and/or areas where feature heights exceed 81.6 m, GLAS waveform would truncate, making it inconvenient to derive range information. For this reason, in later operations height extent was increased to 150 m (1000 bins) over land, using a 'waveform compression scheme' (Harding and Carabajal, 2005).

The nominal diameter of a GLAS footprint is 70 m (spaced at 172 m on along the track); however, its size and ellipticity have varied through the course of mission (Pang et al., 2008). It is equally important to note that footprints of laser 3, laser 2 and laser 1 are moderately elliptical, very elliptical and very elliptical with a side-lobe, respectively (NSIDC, 2008). Varying footprint sizes and ellipticity make delineation of the incident area a challenging task and also introduce uncertainties in estimates (Nilsson, 1996). However, contrary to the findings of St-Onge et al. (2003), GLAS commits to horizontal and vertical accuracies of 3.7 m and 10 cm, respectively (Zwally et al., 2002, Junjie, 2008).

For surface ranging, GLAS uses the TOPEX/Poseidon ellipsoid and the Earth Gravitational Model 1996 (EGM96) geoid as reference. Spacecraft position is determined by a dual frequency Global Positioning System (GPS) in International Earth Rotation Service Terrestrial Reference Frame (ITRF). At the same time, pointing information is given by onboard Instrument Star Tracker (IST) and Hemispherical Resonator Gyroscope (HRG). Combination of spacecraft position and the pointing information yield precise location of the illuminated spot in ITRF, which can be translated to geodetic latitude, longitude and ellipsoidal height (Schutz, 2001, Schutz et al., 2005) (see Section 3.3.1). Figure 1.2 gives diagrammatic representation of the footprint location method.

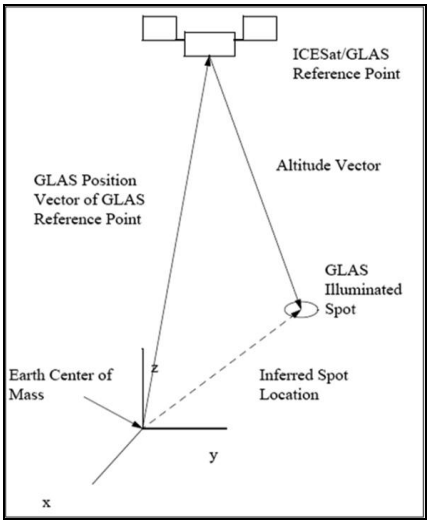

Figure 1.2: Determination of spot geolocation using the resultant vector of position and altitude vectors. Position vector is obtained from Precision Orbit Determination (POD) while the altitude vector is given by Precision Attitude Determination (PAD) of the spacecraft (Schutz, 2002). In cases where no echo is recorded, the geolocation is calculated from predicted orbit, instead of precision orbit, which assumes nadir pointing (NSIDC, 2008).

With this state-of-the-art instrumentation, GLAS acquires global data as a raw waveform (level 0) which is processed by ICESat-Science Investigator-led Processing System (I-SIPS) to produce higher level products (level 1 and 2). Further, from level 0 products, Level 1 A and 1 B products are generated where the latter contains various corrections used to derive level 2 products (Schutz et al., 2005). In total, GLAS offers fifteen data products (GLA01 through GLA15) out of which three (GLA01, GLA06 and GLA14) are of interest in this study (see Section 3.2 for further details).

1.3. Problem statement

GLAS data, due to its unprecedented accuracy, have been used in multiple disciplines which come under the domain of GLAS science objectives (e.g. land topography, cloud heights, hydrology, monitoring of polar ice-sheets, vertical distribution of aerosols and vegetation canopy heights). In this study, vegetation canopy height is of interest which involves processing of level 1 A data product. In studies conducted so far, the underlying assumption is that the transmitted and received signals resemble a Gaussian; and hence use Gaussian functions to decompose the waveform for estimating vegetation height. The ancillary variables accompanying level 1 A product offer a maximum of six Gaussian peaks to be fitted to the waveform (Brenner et al., 2003). However, six modes may not be sufficient to fit the waveform and will lead to discrepant information. Figure 1.3 depicts the actual waveform (top) and six Gaussians (shown in red) fitted to it (bottom), where

the last mode (in red circle) is not captured. The last mode is vital because, principally, canopy height is the distance defined by the time difference between the signal start after noise and the centroid of the last peak (Sun et al., 2008).

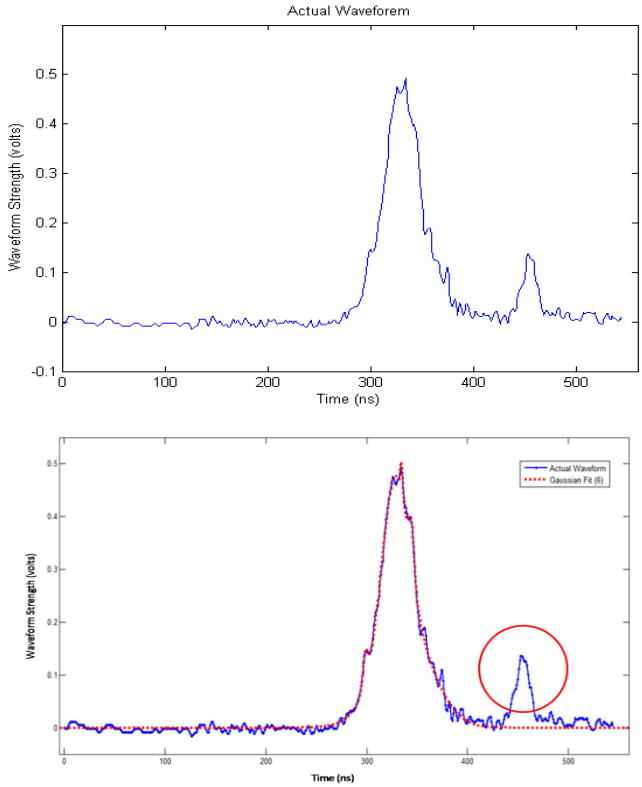

Figure 1.3: Possible discrepancy in Gaussian fitting, where last peak (in red circle) of the waveform is not captured

In similar cases, there is a need to explore robust possibilities of signal processing in order to capture useful information carried by the waveform. This will allow accurate retrieval of canopy height and decrease uncertainties in modelling other variables such as AGB and the amount of carbon in it.

Furthermore, as explained earlier, level 1 B product contains various corrections which are used to derive level 2 products. Apparently, it can be assumed that level 2 products have enhanced accuracy as compared to level 1 B data because of the applied corrections. Thus far, comparison of these two products has not been documented, which asserts their in-depth investigation. This comparison will provide useful insights about the suitability of these products for DEM generation.

Besides, studies on comparison of GLAS/ICESat with its airborne counterpart are still underway. Recent studies on LiDAR, for example Duong et al. (2007) and

Kurtz et al. (2008), present comparative analysis of airborne and spaceborne LiDARs. However, validation of similar studies using ground data is yet a rare attempt.

Significance of canopy height demands its accurate quantification and understanding, especially from GLAS (because of its accuracy and global coverage). In this context, **evaluating the potential of GLAS to estimate canopy heights has been set as the main aim of this study**, which is further divided into specific objectives. Objectives and associated research questions of this study are given below:

1.3.1. Research objectives and questions

1.3.1.1. To investigate the accuracy of level 1 B and level 2 altimetry products in comparison to reference data

Research questions:

a. How consistent are GLAS elevations with the ground elevations?
b. What are the conditions affecting the accurate height estimation from GLAS data?
c. Which data product (level 1 B or level 2) has a higher correlation with the reference data under different topographic conditions?

1.3.1.2. To develop a new methodology which accounts for the discrepancies in canopy height estimation

Research questions:

a. What are the uncertainties involved in canopy height estimation?
b. What are the possibilities of analyzing the LiDAR waveform?
c. How can ground be detected from raw waveform (level 1 A)?
d. What is the accuracy of height estimates as compared to the field data?

1.3.1.3. To compare the performance of airborne and spaceborne LASER altimeters in estimating canopy height, under the same geographical and environmental conditions

Research questions:

a. Are the two datasets spatially coincident and cover the same area?
b. Which dataset (airborne or spaceborne) has higher correlation with the reference data?

1.3.2. Research approach

The general research approach followed to meet the abovementioned objectives is shown in Figure 1.4.

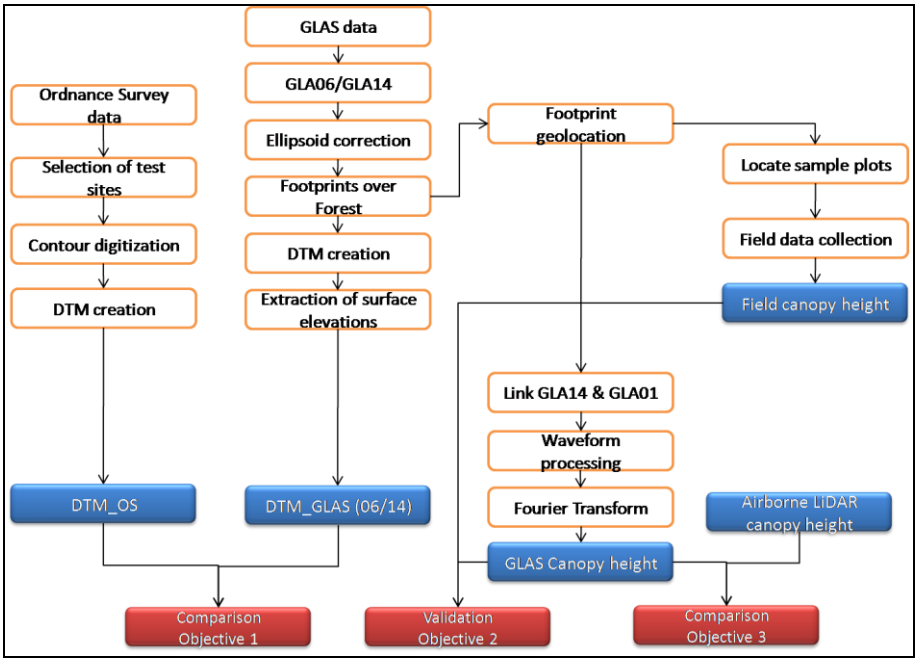

Figure 1.4: General work flow of the study

2. Literature review

Realization of the role of forests in global climate has incited the need of qualitative and quantitative analysis of forest structural parameters for scientific management (Kwak et al., 2005). Structural parameters include canopy height, crown closure, Diameter at Breast Height (DBH), tree volume, basal area and biomass. Existing remote sensing techniques have limited capability to exploit the relationship between canopy height and the remaining parameters (Popescu et al., 2004). Laser altimetry has supplemented the existing remote sensing techniques because of its high precision and capability to estimate canopy height. Moreover, all LiDAR systems provide information on canopy, as well as, subcanopy level which is crucial for understanding forest health and regeneration capacity (Stone et al., 2000, Todd et al., 2003), forest fires (Andersen et al., 2005, Riaño et al., 2003) and present and future carbon accounting (Dean et al., 2004).

2.1. Airborne LiDARs in Forestry

Research on LiDARs for forest inventory started in early 1980s (Hyyppa et al., 2004), which focused mainly on tree heights, species composition, stand density and biomass estimation. Such studies led to the practical application of discrete-return small-footprint airborne LiDARs in forestry during the next decade. It is worth mentioning that earlier Airborne Laser Scanning (ALS) systems separately recorded the first and last returns (Hyyppa et al., 2004). However, the currently available systems do it simultaneously, and more advanced systems can efficiently record up to 5 returns from illuminated surfaces (Leckie et al., 2003). The number of laser shots per squared meter is referred to as point density and is directly proportional to the resolution. This means that high point density will have finer resolution, offering better representation of the target. Pulse repetition frequency, on the other hand, refers to the number of shots fired per second by the laser instrument. The swath width of a laser is defined by the scan angle of the sensor. Diameter of the laser spot, the footprint size, is defined by the beam divergence (in milliradians) and the flight height. Accuracy of LiDAR data depends on point density, scan angle, pulse repetition frequency and nature of incident surface (Hyyppa et al., 2005).

In forested areas, LiDAR pulses represent the vertical strata between canopy top (first return) and ground (last return). Typically, two variables are extracted from laser scanner data: 1) Digital Surface Model (DSM) from the first return which represents the crown surface and 2) Digital Terrain Model (DTM), from last return, representing the ground (Hyyppa et al., 2004). The difference between DTM and DSM, results in the so called canopy height model (CHM). Stand-wise mean canopy height can be obtained from CHMs in many ways, e.g. by applying different statistical operations like simple and weighted averages (Næsset, 1997a) and

percentiles (Magnussen et al., 1999). Because height is more precisely estimated than other canopy parameters, it is preferably used in tree growth studies and the associated changes (Kato et al., 2009).

Increased pulse frequency and higher point densities allow more detailed parameterization of forest attributes, particularly, at an individual-tree scale. Because LiDAR data provides information in three dimensions, canopy heights and their locations can be estimated from CHMs using 'local maximum' filtering approach (Popescu et al., 2002). Also, image segmentation techniques can be applied on rasterized point cloud to delineate tree canopies and estimate their diameter, area and location (Hyyppa, 2000). DBH is reported to have a correlation with both crown diameter (Hemery et al., 2005, Ilvessalo, 1950) and height (Hyyppae et al., 1999, Kwak et al., 2005). Based on this relationship, stem diameter is estimated from crown diameter and tree height using regression models. Further, from stem diameter and height, other variables like basal area, volume and biomass can be worked out (Hyyppa, 2000, Lefsky et al., 2002a, Næsset, 1997a, Lefsky et al., 1999, Lucas et al., 2008). Individual tree parameters are then extrapolated to get stand-level variables.

2.2. Problems with airborne LiDARs

Several studies have achieved good agreement between LiDAR-derived and ground-based estimates, although they are site, instrument and species specific (Lovell et al., 2005). It should be noted that the accuracy of CHM is influenced by errors in both DTM and DSM which has been quantified in many studies e.g. Gaveau and Hill (2003), and Hyyppa et al. (2001).

Forest canopy and subcanopy vegetation intercepts most of the laser pulses, resulting in lesser penetration to the ground surface. This complicates the retrieval of DTMs from airborne LiDAR data, especially in forested environment (Kraus and Pfeifer, 1998, Takeda, 2004). In dense forests, Takeda (2004) reported errors up to 10-20 meters in DTM estimation. Different data processing techniques, however, have effect on these accuracies (Sithole and Vosselman, 2004). Moreover, due to low point density, it was noticed that the LiDAR derived mean canopy heights were underestimated (Aldred and Bonnor, 1985). With low sampling density, probability of the laser to hit the canopy top is lower than hitting the 'tree shoulder' which introduces biases in DSMs (Lefsky et al., 2002b).

In relevance to this study, limitations of airborne systems are divided under three headings, which loosely follow the classification of LiDARs by Dubayah et al. (2000):

2.2.1. Nature of echo recording

Advanced airborne LiDARs are capable of recording up to 5 returns from incident surfaces such as forests (Leckie et al., 2003). These recorded returns are discontinuous or discrete. Discrete returns are not capable to capture the complete

vertical profile of canopies and the resulted representation is at lower resolution. For this reason, vertical profiles generated from airborne data are reported to have possible biases (Harding et al., 2001, Lovell et al., 2003). Alternatively, full-waveform has detailed record of the vertical architecture of vegetation; therefore, increasing confidence in assessment of subcanopy elements (Lee and Lucas, 2007).

2.2.2. Footprint size

Airborne laser scanners have a footprint size in order of few centimetres and are referred to as small-footprint LiDARs. Although small-footprint LiDARs have demonstrated success in forestry applications, larger footprints will enhance accuracy of the estimated parameters e.g. canopy height (Næsset, 1997a). Another factor which has a direct relationship with footprint size is beam divergence. Increased beam divergence is reported to reduce bias in stand height estimates (Aldred and Bonnor, 1985).

2.2.3. Spatial coverage

Due to low flying height, airborne LiDARs have detailed but low spatial coverage. For sites of interest, special flights have to be planned which makes it expensive if investigations are desired many times a year. Cost effectiveness also depends on the spatial extent of an area in question. Regional or global studies with airborne LiDARs will involve high financial inputs. Additionally, on larger spatial scales airborne LiDAR will acquire huge amount of data, processing of which will be extremely time demanding.

Large footprint full-waveform LiDARs account for these limitations, showing increased probability of hitting both the tree top and ground (Mallet and Bretar, 2009). Additionally, they circumvent the biases related to small footprint LiDARs. Earlier experiments on medium footprint (<25 m) full-waveform airborne LiDARs e.g. Scanning LiDAR Imager of Canopies by Echo Recovery (SLICER) (Lefsky et al., 1999) and Laser Vegetation Imaging Sensor (LVIS) (Blair et al., 1999) have shown promise for vegetation characterization on larger extents. However, being airborne, their application is limited to local scales and currently confined to North America (Lee and Lucas, 2007). Global studies on vegetation dynamics necessitate the use of large footprint full-waveform LiDAR aboard a spaceborne platform e.g. Multi-Beam Laser Altimeter (MBLA) and Geoscience Laser Altimeter System (GLAS). The former was part of the Vegetation Canopy LiDAR (VCL) mission which was due to be launched in 2003, but was indefinitely postponed (Mallet and Bretar, 2009). GLAS, on the other hand, was launched in 2003 and offered global coverage until it stopped functioning on October 11, 2009 (NASA, 2009a).

2.3. Spaceborne LiDAR in Forestry

Since its launch, GLAS data have been used in various disciplines e.g. land topography (Carabajal and Harding, 2005, Carabajal and Harding, 2006), cloud distribution (Wylie et al., 2007), hydrology (Carabajal et al., 2006), monitoring of ice-sheets (Kwok et al., 2006, Slobbe et al., 2008), aerosol distribution (Spinhirne et

al., 2005) and vegetation attributes (Harding and Carabajal, 2005, Lefsky et al., 2005, Lefsky et al., 2007). GLAS products, particularly GLA01 and GLA14, have been used for land cover classification and biomass estimation (Boudreau et al., 2008, Lefsky et al., 2005, Ranson et al., 2004), and seasonal changes in vegetation (Duong et al., 2008), where most of the information is retrieved from GLA01 (the 'raw' waveform).

Ranson et al. (2004) explored the capability of GLAS products (GLA01 and GLA14) to classify land cover types on the basis of their response to the incident LiDAR beam. They noted the sensitivity of front slope angle to canopy density and vertical variability of the upper canopy. Front slope angle is the angle, with the vertical, from signal start to the peak of canopy return. It was observed that conifers and mixed forests had higher front slope angles, implicating higher heights due to broadened pulse. On the other hand, smaller front slope angles were showed to indicate lower concentration of the returned energy, which resulted in higher peaks e.g. the ground return.

Also, aboveground biomass estimation has been demonstrated to have agreement with field based or airborne measurements of the same variable (Boudreau et al., 2008, Helmer and Lefsky, 2006, Lefsky et al., 2005). Important variable in biomass estimation is canopy height (Lefsky et al., 2002a) which is commonly reckoned in vegetation studies. Extraction of canopy height from raw waveform is complicated in areas of varied topography due to slope effects (Harding and Carabajal, 2005). Pronounced slopes within the GLAS footprint cause mixing of returns from ground and vegetation canopy, making it difficult to calculate the difference between the two returns.

To account for such complication, Lefsky et al. (2005) derived canopy height as a function of waveform extent and terrain index. Waveform extent was taken as the difference between the first and last threshold crossings of the waveform; whereas terrain index was calculated as the difference between minimum and maximum elevations within a footprint. In order to identify signal start and signal end, certain level of threshold is needed to be applied, which discards noise from the signal. Generally, the histogram method is used for defining threshold level (Helmer and Lefsky, 2006, Lefsky et al., 2005, Sun et al., 2008). In this method, a Gaussian distribution is fitted to the peak of the lowest energies in the waveform. From the Gaussian curve, mean, mode and standard deviation of noise are calculated and used to define the noise threshold level. Further, ancillary data such as DEMs are used to derive terrain indices. Having both waveform extent and terrain index identified, canopy height can easily be modelled. With their method, Lefsky et al. (2005) were able to explain a maximum variation and minimum RMSE of 68% and 4.85 meters in canopy heights. Using a multivariate regression model, aboveground biomass was estimated from GLAS derived canopy height which explained 73% of variance in tropical broadleaved forest. In addition to the regression coefficients of the model, they attributed the unexplained variance in canopy height estimation to the

'measurement' of waveform extent. This underscores the importance of dextrous detection of signal start and signal end, especially the ground return (or peak).

For efficient ground peak detection, Gaussian components are fitted to the raw waveform (Brenner et al., 2003) and iteratively reduced to six (Sun et al., 2008). Harding and Carabajal (2005) suggested that out of the six peaks, the last peak with highest amplitude is a representative of the ground. However, in densely vegetated areas, due to energy attenuation through the canopy (Parker et al., 2001) the ground peak may have lower amplitude than adjacent peaks (Boudreau et al., 2008). In such cases, Boudreau et al. (2008) suggested to consider the peak with highest amplitude as the ground peak, even if it is not the last one. Nonetheless, this will lead to inaccuracies in estimating ground and will, ultimately, be reflected in canopy height. Rosette et al. (2008) reported an underestimation of 1.20 meters in canopy height by considering the first or second highest amplitude peak as ground return.

Height quartiles have also been found as good indicators of forest vertical structure and means of canopy height estimation (Sun et al., 2008). Quartiles H25, H50, H75 and H100 are calculated on the basis of percentage of reflected energy. Quartile H25, for example, represented the aboveground level at which 25 % of the reflected energy is accumulated. Similarly, H100 is the distance between signal start and the ground return, which is in essence the canopy height. Because ground peak is used as a reference for calculating quartiles, it is important to detect the ground peak efficiently.

Sun et al. (2008) presented an automated method for ground peak detection. They used a search window moving from signal end to signal start which would compare the bin values (or signal strength) with the two neighbouring values. If the distance from signal end to the first peak was less than the half width of the transmitted laser pulse, that peak was discarded. In this way, the first 'significant peak' was taken as the ground peak. Their method explained a maximum variability of 83% in canopy height. It should be noted here that signal strength or amplitude of the peaks were not taken into consideration. This automated method may label the first 'significant peak' as ground even if it has a lower energy. Ground or flat surfaces, however, tend to register stronger responses.

Another automated approach for peak identification was proposed by Duong et al. (2008) where a search window of 5 bins (1bin=1ns=15cm) was used. The search window would operate on the normalized and smoothed waveform, moving from beginning through end at a step of one bin. A peak was identified if the central bin had a higher value than the immediate neighbouring bins on left and right, which further had higher values than the two boundary bins. In this way, all major peaks were detected in the waveform. Further, Gaussian components were fitted to the resulting waveform in a way that the minimum distance between neighbouring peaks was 10 bins (1.5 m) and the sigma of an individual peak was 2 bins (30 cm). Also, the number of fitted Gaussian components was limited to six. The last Gaussian mode was considered as the ground return and can be used for determining canopy

height. However, it is reported that some noisier waveforms could not be decomposed by the limited number (six) of Gaussian peaks and such fitting may miss the last mode (Duong et al., 2009). This calls for the need of fitting methods which can circumvent such complexities. Although Gaussian fitting has shown considerable promise in various studies, its efficiency is 'less satisfactory' for pulses with high amplitudes (Wagner et al., 2006). Furthermore, in cases of low amplitude pulses, the extracted parameters are less accurate which demands stringent consideration of the waveform processing algorithms (Mallet and Bretar, 2009).

3. Material and method

3.1. Study area

The study was selected within the New Forest National Park in Hampshire, UK (50^{o} 51' 59" latitude and 01^{o} 40' 50" longitude) covering an area of 29262.36 hectares. This site was designated as Special Area of Conservation in April 2005. Also, it holds the status of Site of Community Importance since December 2004 (JNCC, 2006). Area covered with deciduous broadleaved (oak/beach) and coniferous woodland is 29% and 17 %, respectively. The remaining area is a mix of bogs, marshes, scrub and heath. It is under the active management of the Forestry Commission of Great Britain on compartment and sub-compartment level. A Compartment is a managerial unit which has similar characteristics within the area; such as, soil types, vegetation, productivity and topography (Hubbard et al., 1998). Among others, management objectives of the Forestry Commission include heritage preservation and landscape conservation due to which oak plantations as old as 1810 can be found. Most of the compartments have pure and even-aged stands; however, in some compartments age-diversity exists. In this study, suburbs of the New Forest National Park were also included which were not under the management of Forestry Commission. Figure 3.1 shows the GLAS data projected over the New Forest National Park.

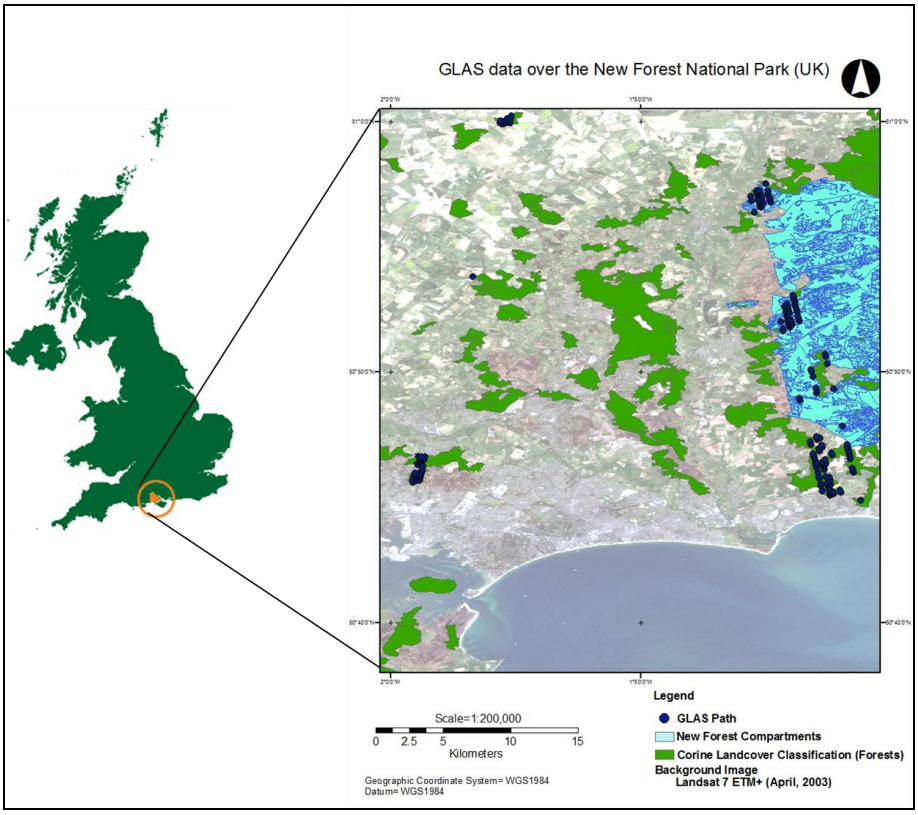

Figure 3.1: Representation of ICESat tracks projected over the study area.

3.2. Description of data

After having the objectives and study area identified, it is important to get acquainted with the data used in this study. The sources from which data were acquired are mentioned in the succeeding text. It should be noted that data were primarily in different reference systems. Necessary description of the data used is given below:

3.2.1. Shuttle RADAR topography mission (SRTM) data

SRTM is an international project mainly lead by National Geospatial-Intelligence Agency (NGA) and the National Aeronautics and Space Administration (NASA). The mission obtained near-global elevation data to generate the most complete high-resolution digital topographic database of Earth (NASA, 2009b). Consultative Group on International Agriculture Research – Consortium for Spatial Information (CGIAR-CSI) provides an easy access to SRTM data at 90 meters resolution. SRTM DEM was procured from the CGIAR-CSI database for the study area. The data were

registered to WGS1984. It is hereinafter referred to as DTM_SRTM and was used to compare its performance against GLAS derived DTMs.

3.2.2. Intermap Digital Terrain Model

Using Interferometric Synthetic Aperture RADAR (IFSAR) technology, Intermap creates digital elevation models for entire UK under its NEXTMap® programme. NEXTMap terrain models commit to 1 m vertical accuracy with 5 m spatial resolution. The data used in this study were already procured from National Environmental Research Council (NERC) Earth Observation Data Centre, through NCAVEO project. The data were registered to Ordnance Survey National Grid. It is hereinafter referred to as DTM_NF and was used to compare its performance against GLAS derived DTMs.

3.2.3. Ordnance Survey Colour Raster Data

Ordnance Survey of Great Britain (OSGB) distributes topographic sheets of various scales through Edinburgh University Data Library (URL1, 2009). For this study, 'colour raster data' scaled 1: 50,000 were obtained in the form of 20 km^2 tiles (each) from the same source. The colour raster maps are generalized products created by cartographers (personal communication Charlotte Phillips, Ordnance Survey). The data give comprehensive landform information, including contours digitized at 10 meters interval with a vertical accuracy of 3 meters (OSGB, 2009). Elevation information retrieved from Ordnance Survey data was used as reference in this study because of its considerable accuracy. The data were registered to Ordnance Survey National Grid.

3.2.4. COoRdinate INformation on the Environment (CORINE) Land cover Classification data

Another dataset used in this study was the CORINE land cover Classification 2000 (CLC2000), which is the European land cover database for the year 2000. In essence, it is a mosaic of national datasets of land cover, categorized into 44 classes under CORINE nomenclature, where the minimum size of a mapping unit is 25 hectares. Based on this dataset, the grid-based product of 100 meters resolution is created by the European Environment Agency (EEA). The latest version (12/2009) of this grid-based product has 'excellent' positional, temporal and thematic accuracies with good completeness and 'excellent' logical consistency (EEA, 2009). From these accuracies of the secondary product, the accuracy of the primary product is evident. The data were registered to European Terrestrial Reference System 1989 (ETRS89). This dataset was used for identifying forest patches in the study area.

3.2.5. Landsat Image

For the purpose of data visualization, a cloud-free Landsat 7 (ETM+) image of April, 2003 was procured from U.S. Geological Survey (USGS) (URL2, 2009). Data are distributed in GeoTIFF format which enables referencing a raster to a known geodetic model or map projection. The image was registered to Universal Transverse

Mercator (UTM) zone 30. True colour composite was used for the purpose of visualization.

3.2.6. Forestry Commission data

The Forestry Commission in England is recognised as international leader in sustainable forestry (FCGB, 2009) which manages timber forests as well as the native woodlands. The New Forest National Park comes under the jurisdiction of Forestry Commission authorities in Hampshire. A database of various compartments under its management is accessible for research purposes which contains necessary information. This includes planting year, area of the compartment, type of species and yield class on compartment as well as sub-compartment level. Data for the study area were collected from Forestry Commission which was registered to Ordnance Survey National Grid. The Forestry Commission has also designed Yield Tables to aid forest management in British conditions (Hamilton and Christie, 1971). From the species-specific Yield Tables and General Yield Class curves, crop height can be estimated if yield class and planting year of the crop are known. Validity of the provided data was confirmed by Forestry Commission authorities (personal communication Jane Smith, FCGB).

3.2.7. Airborne Laser Altimeter data

As one of the study objectives was to compare the performance of airborne and spaceborne LiDARs, results of a study conducted in the New Forest National Park were used for this purpose. The project was carried out at the University of Southampton in 2009, using Leica ALS50-II LiDAR which is a small-footprint discrete-return instrument (Sumnall, 2009). LiDAR data were provided by Natural Environment Research Council (NERC) Airborne Research & Survey Facility (ARSF). After preliminary processing by ARSF, data is delivered to clients. Details of further processing techniques, along with the software packages, can be found on ARSF webpage (URL3, 2009). Since airborne LiDAR data was obtained from a secondary source, it is important to reflect on its quality as follows (see Sumnall (2009) for details).

The data were acquired by NERC research aircraft flown over a subset of 3 x 3 km (in the New Forest National Park) on June 11, 2007 during leaf-on condition. The flight height was about 900 m above ground-level and the instrument operated in 1064 nm channel with a scan angle of 20^{o}. Pulse frequency was 30 kHz and the resulting point density was 1.2 points per m^2. For those points where the difference between first and last return was less than 0.6 m, they were assumed as bare-ground (Sumnall, 2009). After 'filtering' the non-terrain points, DTM was interpolated at 1 m spatial resolution, using Inverse Weighting Data (IDW), resulting in RMSE of about 0.38 m. Further, DSM was created from first return using 3 x 3 low-pass filter for smoothing and 3 x 3 high-pass filter for highlighting boundaries tree crowns. On the rasterized DSM, a set of multi-resolution segmentation techniques was applied to delineate tree crowns as image objects. Maximum height within each crown image object was considered as canopy height. The LiDAR derived canopy heights were within ±3 m of the field measured heights.

3.2.8. GLAS/ICESat data

Out of 15, three data products of release 28 and 29 were used in this study, which were GLA01, GLA06 and GLA14. Data were procured from National Snow and Ice Data centre (NSIDC) through ICESat/GLAS data subsetter (URL4, 2009). It is suggested to refer to the GLAS data as 'Zwally et al. (2006)'. Description of these datasets is as follows:

3.2.8.1. GLA01:

This is level 1A global altimetry product which contains intensities of transmitted and received waveforms. GLAS digitizes these intensities as counts which are afterwards converted to volts (by users) using calibration tables (Appendix-I) in GLA01 header records. Moreover, the transmitted pulses were arranged in time order, which means that the value of the first sample is for the sample closest to the spacecraft in time. Contrarily, the received echo is in time-reversed order, which means the the value of the first sample is for the sample farthest from the spacecraft in time (NSIDC, 2008).

Most importantly, GLA01 stores index number, shot time, shot number, number of shots of the pulse and echo intensity. However, GLA01 also contains information on various variables such as latitude and longitude of the spot from 'Predicted' orbit, peak values of transmitted pulses, type of echo compression and other correction flags. Details of these variables can be found in GLAS altimetry dictionary (NSIDC, 2009a).

3.2.8.2. GLA06:

This is level 1B global elevation data which is derived from GLA01 (actual waveform). The product gives information about surface elevation, surface roughness assuming no slope, surface slope assuming no roughness and atmospheric and geodetic corrections for range measurement. GLA06 is intended for research purposes from which region-specific level 2 elevation products are derived (Brenner et al., 2003). GLA06 is used in conjunction with GLA05 to create level 2 products which are GLA12 through GLA15 (NSIDC, 2008). GLA05 is level 1B waveform-based range correction product containing all parameters of waveform characteristics and those parameters required to calculate physical properties of the surface (Brenner et al., 2003). Elevations are given in meters with respect to a reference ellipsoid accompanied by geoid elevations which allow users to calculate orthometric heights. In addition, various correction flags are also provided with this product at least twice per 40 shots (40 shots make one 'record'). Important flags include saturation elevation correction and gain values used for the received echo. Similar to GLA01, GLA06 also contains geolocation of footprint centroid, unique record and shot numbers, and a time stamp with Universal Coordinated Time (UTC) in J2000 (referenced from noon on January 1, 2000). However, unlike GLA01, geolocation of footprints are determined from 'Precision' orbit for GLA06 and GLA14.

It is important to note that geodetic latitude, longitude and surface elevations from GLAS products are calculated using different methods, i.e. standard parameterization and alternative parameterization. In standard parameterization the driving algorithms are specifically designed for ice-sheets. On the other hand, alternative parameterization refers to calculating geodetic latitude, longitudes and surface elevations using algorithm designed for land (NSIDC, 2008). Surface elevations given by GLA06 have been retrieved using standard parameterization. These elevations are also referred to as ice-sheet specific ranges. Moreover, GLA06 product contains a long list of other additional variables, details of which can be found in GLAS altimetry dictionary (NSIDC, 2009a).

3.2.8.3. GLA14:

This is level 2 region-specific land surface altimetry data which is derived from level 1 products (GLA05 and GLA06). GLA14 has almost the same variables as GLA06 except that GLA14 elevations, geodetic latitude and longitude are calculated using land-specific range. Land-specific range means that these variables are derived using alternative parameterization which uses algorithm specifically developed for land surfaces.

Two important variables associated with GLA06 and GLA14 are saturation elevation correction flag and gain value of the receive pulse. Since GLA14 is a processed product obtained from GLA05 and GLA06, elevation correction is not recommended to be applied to GLA14 (NSIDC, 2008). However, this correction should be added to GLA06 elevations. Gain value of the echo, which ranges from 0-250, indicates the level of pulse saturation. A high gain value refers to high level of saturation; whereas negative gain value (-999) denotes that the waveform is distorted and cannot be used for analysis (personal communication with David Korn, NSIDC). As the transmitted and received pulses are assumed to resemble a Gaussian shape (Brenner et al., 2003), a Gaussian pulse is fitted to the waveform during processing. For this purpose, GLA14 variables also include amplitudes, areas and standard deviations of 6 Gaussians if the user is interested in Gaussian fitting.

It may be noted that GLA01 carries the signal strength while GLA06 and GLA14 contain geolocation of the incident LiDAR beam. The record number, shot time and shot number are common fields across GLAS products which are used for time-stamping raw waveforms. Other variables, of relevance to this study, are described in Table 3.1.

Table 3.1: Summary of GLAS variables used in this study

Output Data Column	Element of	Description
Record Number	GLA01, GLA06, GLA14	GLAS digitizes forty echo signals per second. Each set of forty shots is assigned a unique record number during processing of level 0 data
Shot Number	GLA01, GLA06, GLA14	In each record, there are forty shots and each is assigned a number called the shot number
Date	GLA06, GLA14	Date of transmitted pulse in mm/dd/yyyy format (e.g. 25/10/2003)
Time	GLA06, GLA14	Time of the transmitted pulse in hh:mm:ss.sss format (e.g. 07:57:58.320)
i_lat	GLA06, GLA14	Geodetic latitude of the laser shot in degrees. It has been computed from Precision orbit and Precision attitude. All instrument corrections, atmospheric delays and tides have been applied
i_lon	GLA06, GLA14	Longitude of the laser shot in degrees, computed after all instrument corrections, atmospheric delays and tides have been applied
i_elev	GLA06, GLA14	Surface elevation (in meters) of the laser shot from the reference ellipsoid
i_gdHt	GLA06, GLA14	Height of the geoid above the reference ellipsoid (in meters)
i_satElevCorr	GLA06, GLA14	Correction to elevation for saturated waveforms. High-amplitude returns from flat and/or bright surfaces cause waveform saturation which results in negative surface elevation bias. Saturation elevation correction has not been applied to GLA06, which can be over a one meter correction
i_gval_rcv	GLA06, GLA14	Gain value of the received pulse. It ranges from 0-250
i_UTCTime	GLA01, GLA06, GLA14	Transmit time in UTC of the 1st shot in the 1 second frame referenced to noon on January 1, 2000 (J2000). The first item is the whole number of seconds; the second item is the fractional part in microsecond (e.g. 120340678.321)
i_rng_wf	GLA01	Strength of echo waveform in count which ranges from 0-255
i_Gamp	GLA14	Amplitude of each Gaussian solved for (up to six) waveform processing (in 0.01 volts). These values are derived using alternate parameters
i_Garea	GLA14	Area of each of Gaussian solved for (up to six) waveform processing (in 0.01 volts*ns). These values are derived using alternate parameters
i_Gsigma	GLA14	Width (standard deviation) of each of Gaussian solved for (up to six) waveform processing (in 0.001 ns). These values are derived using alternate parameters

In essence, first objective of this study was comparison of surface elevations derived from GLA06 and GLA14. Due to different parameterization used in obtaining these two altimetry products, their estimated surface elevations do not coincide. Even the same spot location has height variation because of the different methodologies

involved. In order to meet this objective, both GLA06 and GLA14 data were compared with the reference data (OSGB). In addition, comparative analysis of two other elevation products (i.e. DTM_SRTM and DTM_NF) was also performed relative to OSGB data. This informed on the accuracy of GLAS data with respect to other available elevation products. For this purpose, digital terrain models were created from GLAS point elevations.

Similarly, for objective two a methodological approach was adopted to extract tree heights. This approach involved waveform processing using Fast Fourier Transform. Due to the possibility of Gaussian to leave out the last peak of the signal, Fourier method was applied to capture all major peaks and circumvent the intricacies involved. Field data were required for validation of the new method. GLAS footprints, for which field data were not available from other sources, were visited to collect the same.

Realizing the need of comparing GLAS results, from the second objective, with its airborne counterpart, it was addressed by the third objective.

3.3. Methodology

The methodology was divided into four phases as shown in Figure 3.2:

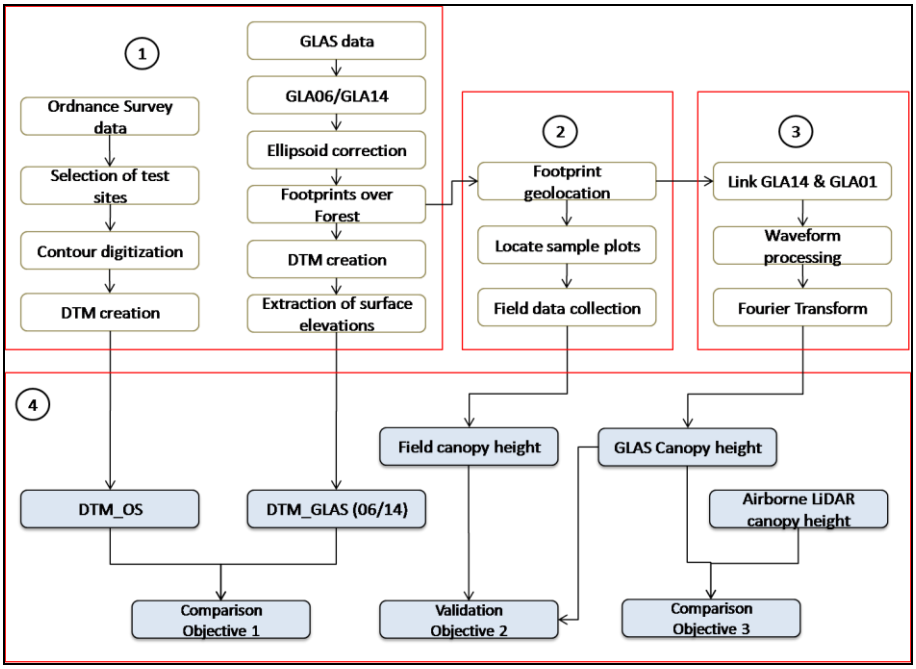

Figure 3.2: Breakup of methodological steps is shown in red boxes: 1) Data pre-processing, 2) Field work, 3) Waveform processing and 4) final Data analysis. Details of step 3 are given in its respective section.

These phases (shown in Figure 3.2) are described in detail as follows:

3.3.1. Data pre-processing

It should be noted that the datasets used in this study were registered to different reference systems. To have the datasets coherent, they were all re-projected to a common reference system, the World Geodetic System 1984 (WGS1984).

3.3.1.1. Extraction of GLAS Elevation data (GLA06 & GLA14):

The elevation products (GLA06 and GLA14) are distributed in binary format (*.DAT) which were converted to ASCII format. Moreover, GLAS elevations are referenced to the TOPEX/Poseidon ellipsoid which is 70 cm smaller than WGS84 ellipsoid. For GLAS data to be coherent with the other datasets used in this study, ellipsoid correction from TOPEX to WGS84 was applied. This correction is necessary to augment the latitudinal and elevation accuracy. For all these conversions Interactive Data Language (IDL) programmes, developed by NSIDC (NSIDC, 2009b), were used. As latitudinal and longitudinal information give point locations, they were buffered to footprints using footprint information. Depending upon the varying footprint sizes of GLAS lasers (1, 2 and 3), different sizes of buffers were used (Table 3.2). Further, by subtracting geoid height from corrected surface elevation, orthometric height of each footprint was calculated.

3.3.1.2. Extraction of GLAS Waveform data (GLA01):

GLA01 waveforms are originally in counts which were converted to voltages using IDL codes provided by National Snow and Ice Data Centre (NSIDC, 2009b). The codes utilize calibration tables (Appendix-I), available in GLA01 header, for this conversion. GLA01 waveforms were then linked to GLA14 on the basis of record and shot numbers. To continue, GLAS footprints over the study area were identified and waveforms with high level of echo saturation were filtered out. Further, CORINE land cover classification was used to identify forest patches in the study area and extract GLAS footprints over forest were extracted for further analysis. The total number of footprints over forests was 202. As GLAS collects data three times a year for about a month long period, it is designated with respective month, year and the laser used. GLAS data used in this study along with its relevant details are given in Table 3.2.

Table 3.2: GLAS data used in this study with its year and campaign identity

S. No.	Data Year	Month	Laser Campaign	Footprint Size (m)*	Number of Footprints
1.	2003	October	L2A	73.5	36
2.	2004	February	L2B	73.5	25
3.	2004	May	L2C	73.5	16
4.	2004	October	L3A	54	23
5.	2005	February	L3B	54	05
6.	2005	May	L3C	54	25
7.	2006	March	L3E	54	02
8.	2006	June	L3F	54	37
9.	2006	November	L3G	54	33
				Total	**202**

**averages of semi-major and semi-minor axes (L2=95&52, L3=61&47)*

It is important to mention that the footprints used for evaluating elevation (GLA06 and GLA14) and altimetry (GLA01) products were not necessarily the same. If generalized, the study area had eastern and western GLAS tracks. Due to accessibility issues, only eastern tracks were used for waveform analysis, which comprised of 145 footprints.

3.3.1.3. Digital Terrain Models:

For comparing GLAS elevations with Ordnance Survey elevations, digital terrain models of 2 m resolution were interpolated from GLAS point elevations (DTM_06 and DTM_14). Two small test sites, within the study area, were selected as representatives of low and high lying topography. Also, the site with higher elevations was covered with dense forest. Location of these two test sites is shown in Figure 3.3.

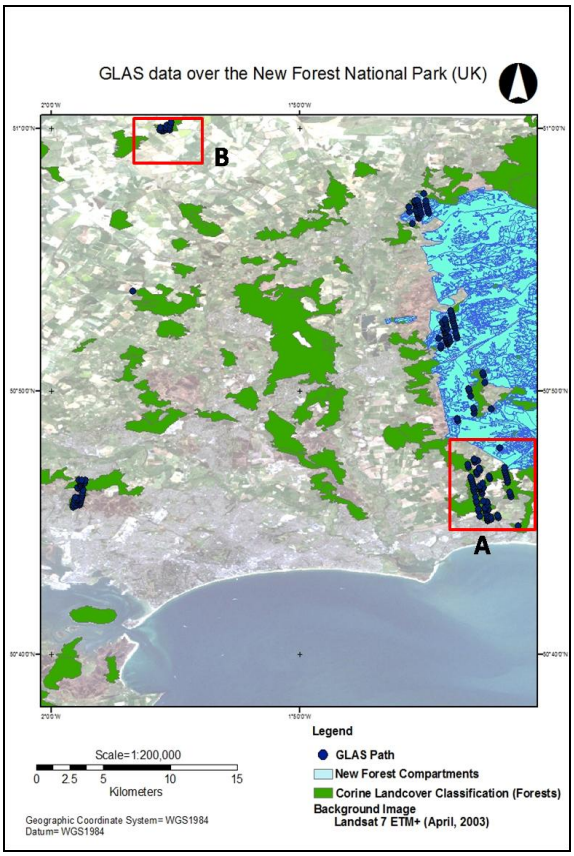

Figure 3.3: Selected sites for comparative analysis of GLA06 and GLA14 elevation products. Test Site A covered the coastal plain; whereas, Test Site B was covered with dense forest. Due to lesser GLAS coverage, test site B has a smaller area.

Furthermore, DTM_SRTM and DTM_NF were resampled to 2 meters spatial resolution. Since GLAS gives mean elevation of the footprint, 2 meters resolution for these terrain models was chosen so that their mean elevations within the incident beam can easily be worked out. Similarly, contours from the Ordnance Survey colour raster were digitized and interpolated to create digital terrain model (hereinafter referred to as DTM_OS), with the same spatial resolution, for these test sites. Figures 3.4 and 3.5 show the digital terrain models of test sites A and B, respectively. Test site B did not have DTM_NF coverage.

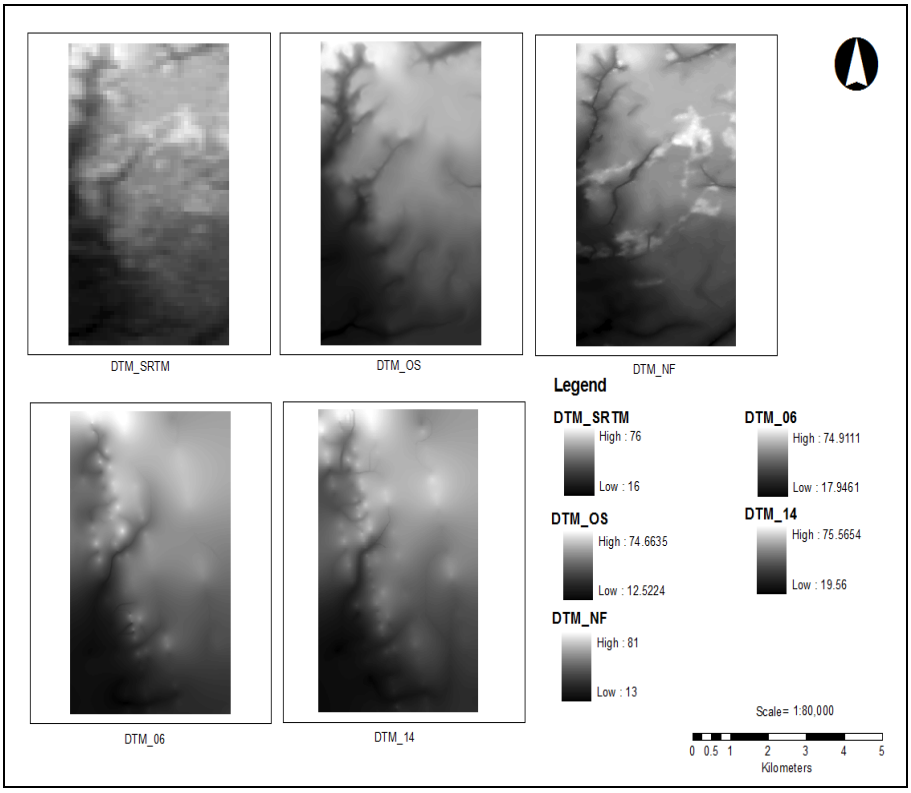

Figure 3.4: Digital terrain models of Test Site A, with spatial resolution of 2 meters (Area= 16.25 km^2).

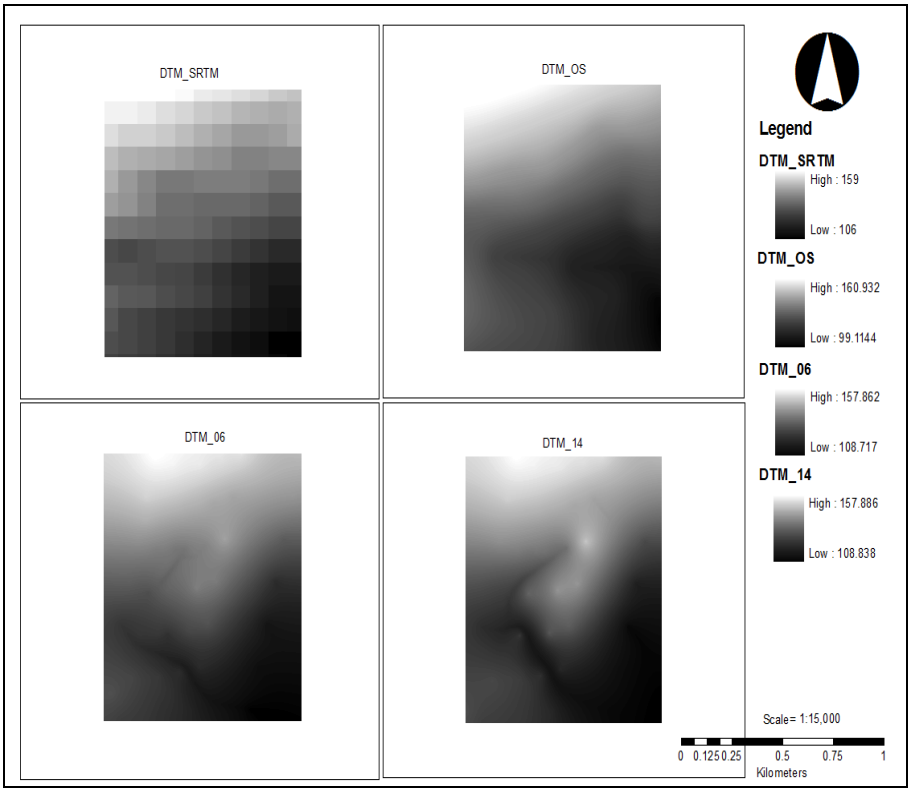

Figure 3.5: Digital terrain models of Test Site B, with spatial resolution of 2 meters (Area= 0.65 km^2).

Using GLAS footprints, the mean elevations within footprints were calculated from different terrain models and compared with DTM_OS. Coefficient of correlation was used as indicator of goodness of fit; however, to quantify the uncertainty, root mean squared error was used.

3.3.2. Field work

Before proceeding with the field work, it was important to identify the footprints which will be sampled for canopy height estimation. Out of 145, 50 points were randomly selected for field data collection to avoid bias and obtain representative samples (Lefsky et al., 2005). Further, out of these 50 identified points, 23 fell in the management boundaries of the New Forest National Park for which the Forestry Commission data was readily available. For the remaining 27 points, field work was conducted in mid-October, 2009. Along with any field work comes the issue of inaccessibility. Four footprints falling on privately owned agricultural lands could not be visited. In addition, 03 footprints were over peat bogs and one over a blank area. In the remaining 19 footprints, canopy heights were recorded. Figure 3.6

illustrates the distribution of field measurement, Forestry Commission and inaccessible GLAS points.

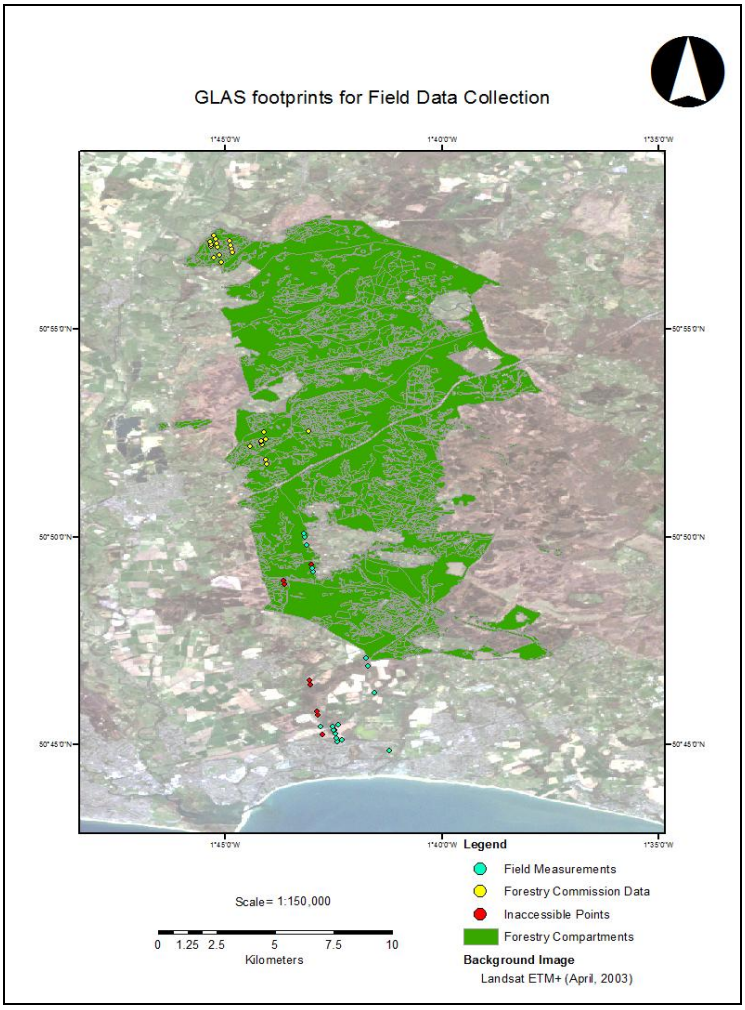

Figure 3.6: Representation of GLAS footprints selected for field data collection using random sampling

Details of these selected footprints are presented in Table 3.3.

Table 3.3: Summary of footprints used for waveform analysis

	Data Year	Month	Laser Campaign	Number of Footprints
Field Measurements	2003	October	L2A	5
	2004	February	L2B	4
	2004	October	L3A	1
	2005	May	L3C	2
	2006	June	L3F	3
	2006	November	L3G	4
Forestry Commission	2003	October	L2A	4
	2004	February	L2B	1
	2004	October	L3A	1
	2005	May	L3C	8
	2006	June	L3F	5
	2006	November	L3G	4
Inaccessible	2003	October	L2A	1
	2004	October	L3A	7
			Total	**50**

A handheld Garmin eTrex GPS receiver was used, with an accuracy level of 7 meters or below, to locate the footprint centres. Within each footprint, angle of elevation (top) and depression (base) of trees greater than 10 cm DBH were recorded with a clinometer. Also, horizontal distance from trees, ground elevations, species and description of footprint were recorded in the 'field data form' (Appendix-II).

Data collection was flexible in terms of the sample size; however, variability was taken care of. In compartments with homogeneous cover, fewer trees were measured than in uneven-aged plots. In uneven-aged areas, within footprints, data was collected in 4 annular plots, one in centre and three on the footprint margin at approximate azimuths of 0^o, 120^o and 240^o. Radius of central plot was 10 meters while the radii of smaller marginal plots were 5 meters each. Radius of the central plot was kept more than the marginal ones, to account for the reflected LiDAR energy which has a central maximum and fades away radially outwards (Duong et al., 2006b). Figure 3.7 gives the conceptual sampling design for a footprint.

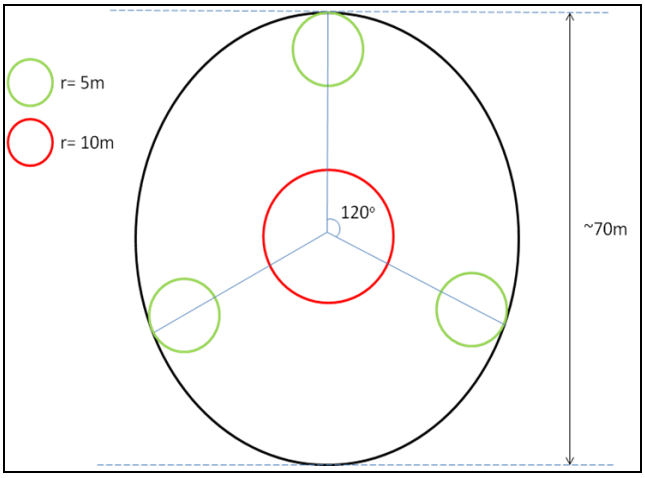

Figure 3.7: Conceptual layout of sample plot for measuring canopy heights in the field

3.3.3. Waveform processing

This section forms the core of this study where application of a new method, Fourier Transform, for waveform fitting is introduced for obtaining canopy heights.

3.3.3.1. Fourier Transform:

Fourier transform is a combination of analysis and synthesis of a wave. It converts the waveform from time domain to frequency domain and decomposes it into two components, i.e. the real and the imaginary part (cosine and sine, respectively). A spectral estimator is used to measure the signal strength per unit of frequency. Power Spectral Density (PSD) was used as a spectral estimator, which was in angular units (radians), to find the region of maximum signal strength. The angular units (ω) were converted to the number of waves (harmonics) using equation 3.1, which represented the signal strength.

$$\omega = 2\pi/T \qquad (3.1)$$

where, ω is power per unit frequency, $2\pi=360^{o}$, T is the time duration. The number of harmonics was used for synthesizing back a waveform from the decomposed one.

Figure 3.8 and 3.9 exemplifies the PSD analysis. Figure 3.8 shows an actual waveform in time domain over which PSD analysis was performed. Figure 3.9 shows the decomposed waveform in frequency domain where the red dotted line (at 15^{th} frequency) marks the range of maximum signal strength.

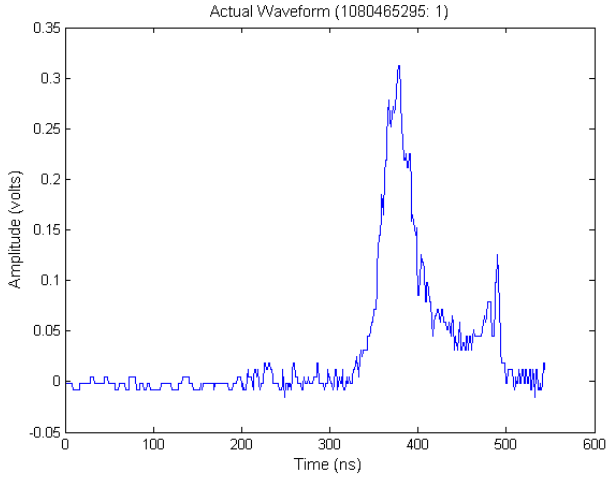

Figure 3.8: Actual waveform in time domain

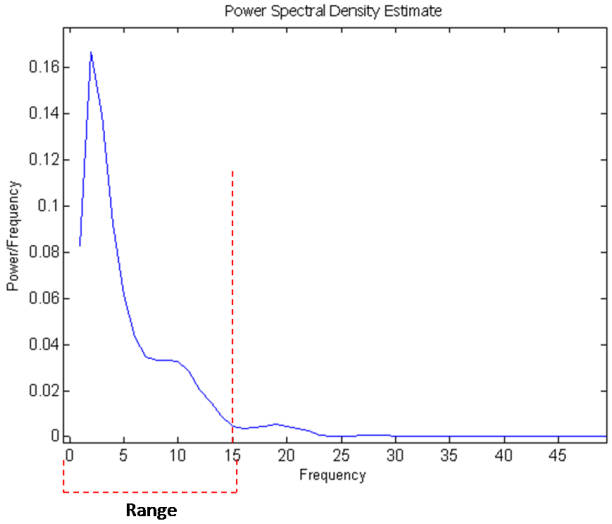

Figure 3.9: Decomposition of waveform in Figure 3.8 into frequency domain, using PSD analysis. Red dotted lines mark the range of maximum signal power. The signal has been zoomed for better visualization

By substituting 15 in equation 3.1, we get 24 harmonics in this particular case, which will be used for synthesizing the fitted waveform.

As canopy height is the distance between signal-start after noise and the centroid of the last peak, it was crucial to detect these points efficiently. A MATLAB code was used to identify waveform parameters, which was developed by Dr. Jadunandan Dash. Various steps, taken to arrive at canopy height estimation (Figure 3.10), are as follows:

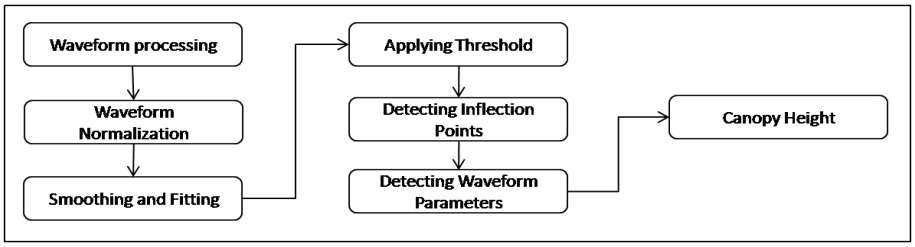

Figure 3.10: Flow diagram of waveform processing

3.3.3.2. Waveform Normalization:

Since different waveforms have different amplitude intensities, it is inconvenient to apply a single threshold value to all waveforms. Figure 3.11 shows two different waveforms on the same scale. Due to difference in amplitude intensities, a single threshold value cannot be used for noise discrimination.

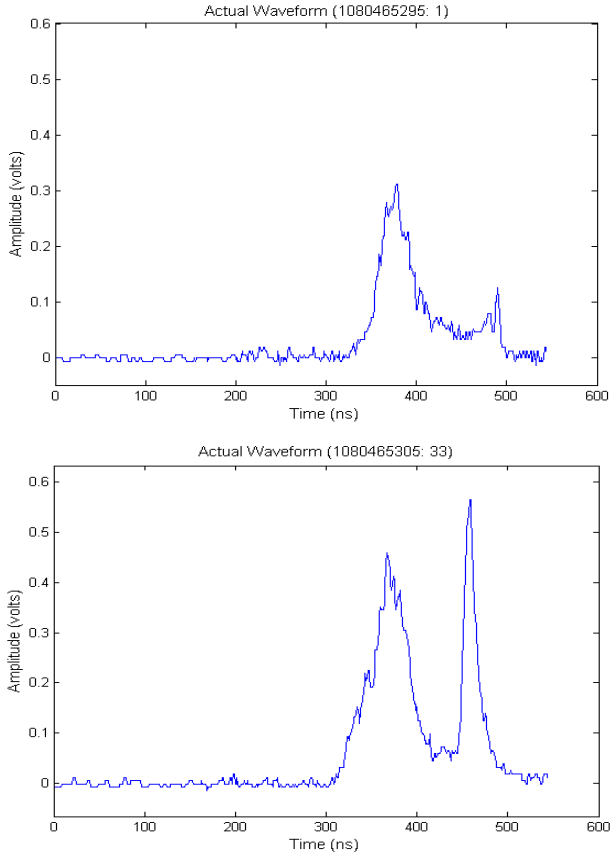

Figure 3.11: Comparing two waveforms before normalization

Waveforms digitized at different times can be compared after they are normalized. This was achieved by dividing the received energy at each instance (E*i*) by the total received energy (ET) , where total energy is $\sum_{i=1}^{544} \mathbf{E}_i$ (Duong et al., 2006a). Mathematically, it is expressed as:

$$Normalized\ waveform = Ei / \sum_{i=1}^{544} \mathbf{E}_i \qquad (3.2)$$

Having normalized the waveforms as shown in Figure 3.12, their comparison and processing is convenient, especially in defining the noise level.

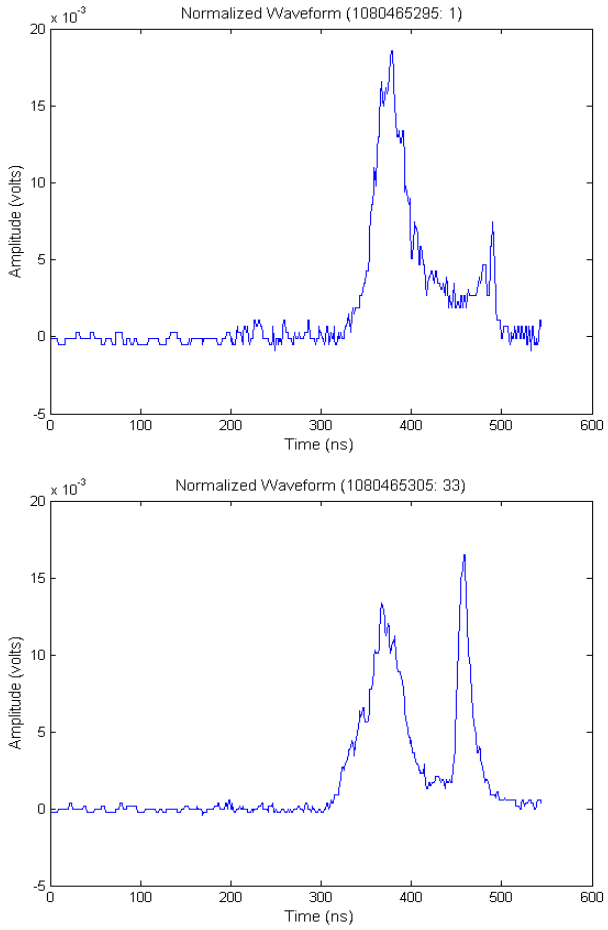

Figure 3.12: Comparing two waveforms (from Figure 3.11) after normalization

3.3.3.3. Waveform smoothing and fitting:

The normalization step was followed by smoothing the normalized waveform and fitting a modelled waveform to it. For this purpose, Fast Fourier Transform (*fft* function in MATLAB) was used which is an efficient algorithm (Zadiraka and Igisinov, 1973) to compute discrete Fourier transform (analysis) and its inverse (synthesis). The number of harmonics, in essence, is the number of fitted peaks to the actual waveform. In this study, 30 harmonics were used for smoothing of and model-fitting to the normalized waveform. Figure 3.13 shows the normalized waveform (top) in blue along with the Fourier fitted waveform (bottom) in red.

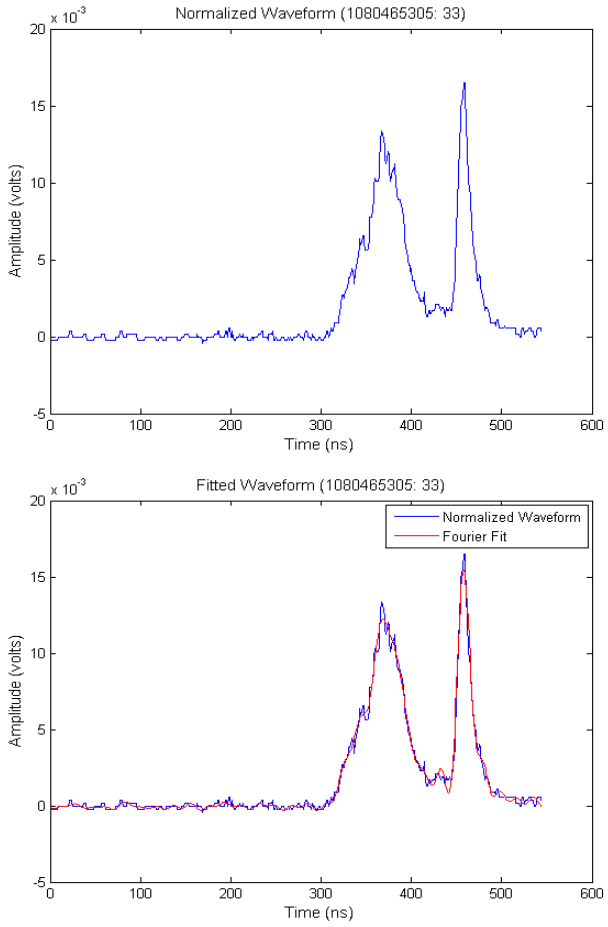

Figure 3.13: Normalized waveform before (top) and after (bottom) Fourier fitting

Fundamentally, frequency domain was obtained from time domain using the Fourier algorithm as given in equation 3.3:

$$f(t) = a_0 + \sum_{n=1}^{544}(a_n \cos n\omega t + b_n \sin n\omega t) \quad (3.3)$$

Where, a_0, a_n and b_n are the coefficients of amplitude of the fitted wave (sinusoids), *n* is the number of time instances and *t* is the position of respective fitted wave.

3.3.3.4. Threshold and background noise:

The GLAS echo telemetered in 544 bins corresponds to a height of 81.6 meters over land. Out of 544, the first 200 bins (30 m) were used to define the noise level. The remaining 344 bins (51.6 m) were sufficient to represent the vegetation structure without truncation. A noise threshold level was used to single out the signal from noise and identify locations of signal-start and signal-end. Start and end of the signal are threshold crossings of the leading and trailing edges (Harding and Carabajal, 2005). As stated in Lefsky et al. (2005), the threshold level was set to the sum of mean noise and 4 times the noise standard deviation. The resulting waveform from this step is shown in Figure 3.14.

$$\textit{Threshold level= mean noise + 4* noise standard deviation} \quad (3.4)$$

In this study, the first 200 bins were used to calculate the threshold parameters as shown below:

$$\textit{Mean noise} = \bar{E} = \sum_{i=1}^{200} E_i/200 \quad (3.5)$$

$$\textit{Noise standard deviation} = \sqrt{\sum_{i=1}^{200}(E_i - \bar{E})^2/200} \quad (3.6)$$

Where, E_i is the received energy at time *i*.

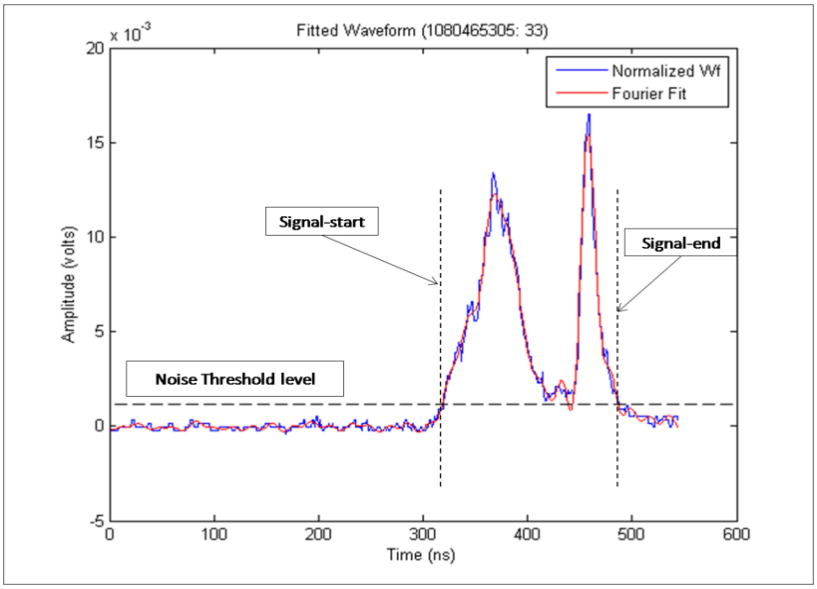

Figure 3.14: Using a defined threshold level to discriminate between noise, signal-start and signal-end (as in equation 3.4)

3.3.3.5. Identification of peak locations:

Most important was the detection of points of inflection, from which other variables like ground, canopy top and canopy height can be worked out. First, all peaks were identified by a search window (1 nanosecond) which moved from start to end of the waveform. The window calculated the difference between two succeeding amplitudes, and stopped until it found the point where the first derivative changed from positive to negative or vice versa. In this way, all the peaks and troughs were identified and marked as shown in Figure 3.15. Further, the peak with maximum amplitude was observed, which was used for ground, canopy point, canopy top and finally canopy height.

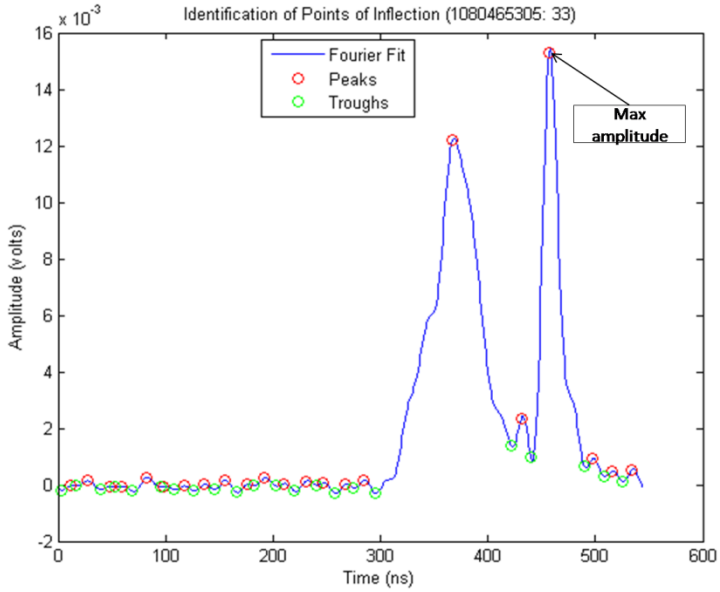

Figure 3.15: Identified peaks (in red circles) and troughs (in green circles) on the fitted waveform. Peak with maximum amplitude is also marked for determining ground, canopy top and canopy height.

3.3.3.6. Detecting Ground, Canopy-top and Canopy height:

To detect these parameters, the maximum amplitude was used as a reference. From this point, the window moves towards the signal-end and searches for a ground return peak. Peak with amplitude one-fifth the maximum amplitude, above the defined threshold, was detected as the ground return. It was assumed that due to reduced penetration and decay of energy through the canopy (Parker et al., 2001), the return energy can be as low as one-fifth of the maximum amplitude. If these conditions were not met, the maximum amplitude peak was designated as the ground return.

After detecting ground, again, the window moves from the maximum amplitude peak towards the signal start to search for canopy point. Canopy point is defined here as the first peak after the signal-start which is above the threshold level. Leading edge of the canopy point indicates the canopy-top, because as soon as the signal interacts with the uppermost foliage and/or branches, it is excited. Further, canopy height was calculated as the distance between ground return and canopy top (Figure 3.16). In case the ground return and the canopy top peaks coincided, the canopy height was zero.

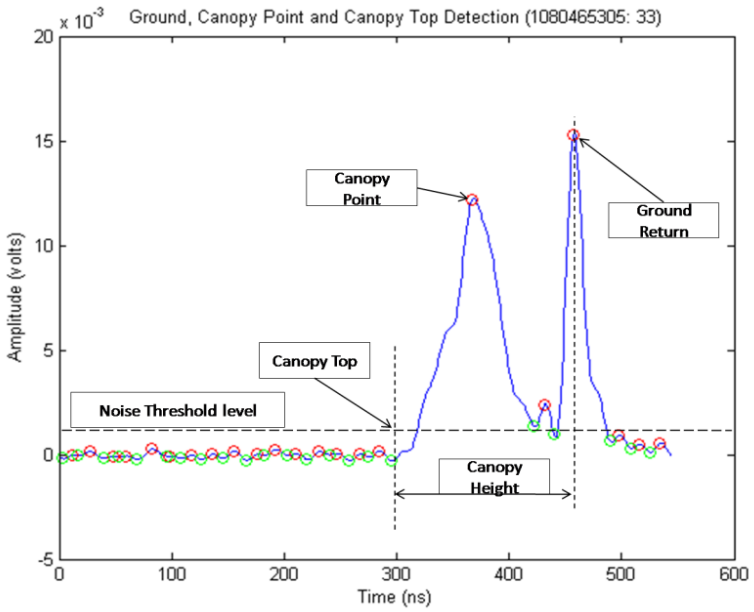

Figure 3.16: Representation of final parameter detection (using the MATLAB code). Red and green circles show the waveform peaks and troughs, respectively.

Similarly, canopy heights were calculated from all selected waveforms and compared with their respective field data using coefficient of correlation. Heights retrieved from GLAS were also compared with the airborne laser altimeter data.

3.3.4. Data analysis

Surface elevations from different DTMs were categorized into three classes which are described below:

a) Accurately estimated elevations: Elevations with ±2 meters difference from DTM_OS
b) Over estimated elevations: GLAS elevations are above 2 meters from DTM_OS
c) Underestimated: GLAS elevation are below -2 meters from DTM_OS

Angles of elevation and depression of tree top and bottom (respectively), and distance of tree from the point of observation were used to calculate tree heights (equation 3.7).

$$\textit{Canopy height (field)} = d*\tan\theta + d*\tan\Phi \qquad (3.7)$$

Where, d is the distance between the tree and the point of observation (in meters), θ is the angle of elevation of the canopy top in degrees, and Φ is the angle of depression of the tree bottom in degrees. Because the waveform is sensitized by the

uppermost foliage and/or branches, it represents the maximum canopy heights inside the footprint. For this reason, field canopy heights of dominant trees were used for analysis. Moreover, there was a time lag between GLAS acquired data (see Table 3.3) and field collected data, during which heights increments were expected. Annual height increments for each species were worked out from yield tables and subtracted from field calculated canopy heights, to get adjusted canopy heights.

Canopy heights for the footprints falling in Forestry Commission sub-compartments were estimated from Yield Class curves in Hamilton and Christie (1971). Forestry Commission data contained planting year and yield class on sub-compartment level. Crop age was estimated as the difference between planting year and GLAS data acquisition year. With these parameters at hand, canopy height was worked out as shown in Figure 3.17. Crop Yield classes are illustrated in red box. The red dotted lines show the intersection (at red cross) of age-axis and the Yield class. Canopy height can readily be obtained from the vertical axis. In Figure 3.17 Yield class 12, for example, refers to timber volume of 12 m^3/year/hectare.

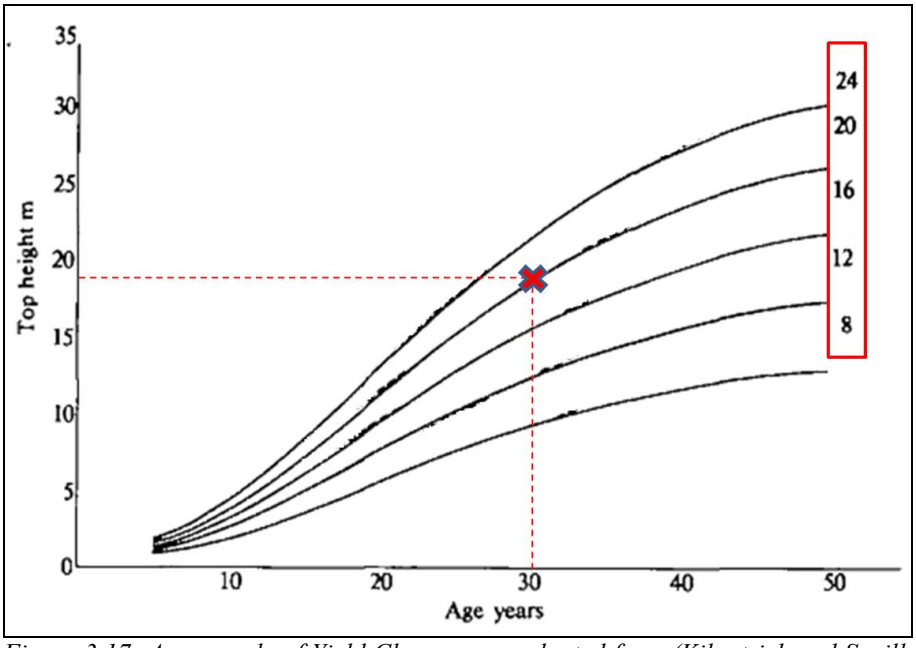

Figure 3.17: An example of Yield Class curves adapted from (Kilpatrick and Savill, 1981).

Maximum height (e.g. 18 m in Figure 3.17 for a crop with 30 years of age and Yield class 16) was taken as canopy height of the sub-compartment.

As the study involved comparative analysis and validation, scatterplots were used to display the relationship between two quantitative variables. This was to visualize the overall form of relationship and look into striking deviations, if any. Further,

Pearson's coefficient of correlation (R) was used as a numerical supplement of linear relationship between two datasets. Nevertheless, R-value does not inform on the magnitude and direction of associated errors. For this purpose, root mean squared error (RMSE), which is the absolute measure of the distance between the estimate and the reference (Sumnall, 2009), was calculated to quantify these errors.

4. Results and discussion

Two tailed Pearson's correlation in Statistical Package for Social Scientists (SPSS v.16) was used to compare any two datasets resulting from the adopted methodology. Scatter plots were produced with the same software package for analysis. R-value and RMSE were used as indicators of 'goodness of agreement' between corresponding variables. For the purpose of convenience, objective-wise results are presented in this section, followed by respective discussion.

4.1. Relationship of GLAS elevation products

Results of correlation of different DTMs used in this study with the Ordnance Survey DTM (DTM_OS) in Test Site A are shown in Figure 4.1 (a, b, c & d). All four figures are captioned under Figure 4.1 (d).

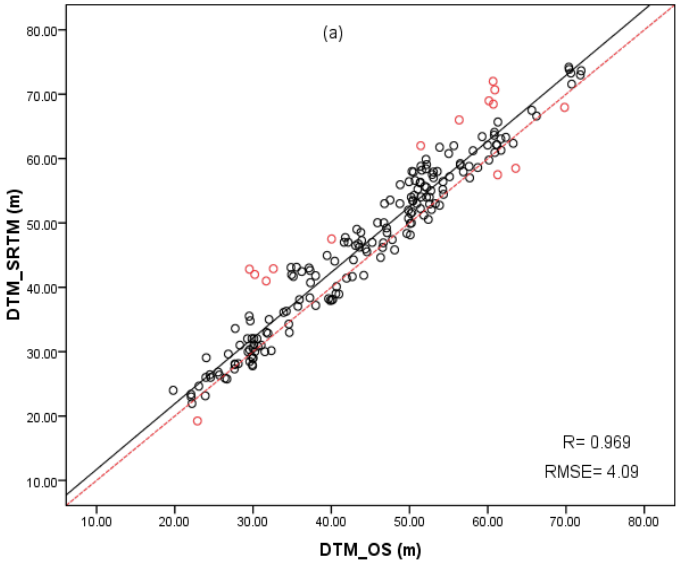
(a)
DTM_SRTM (m)
DTM_OS (m)
R= 0.969
RMSE= 4.09
10.00
20.00
30.00
40.00
50.00
60.00
70.00
80.00

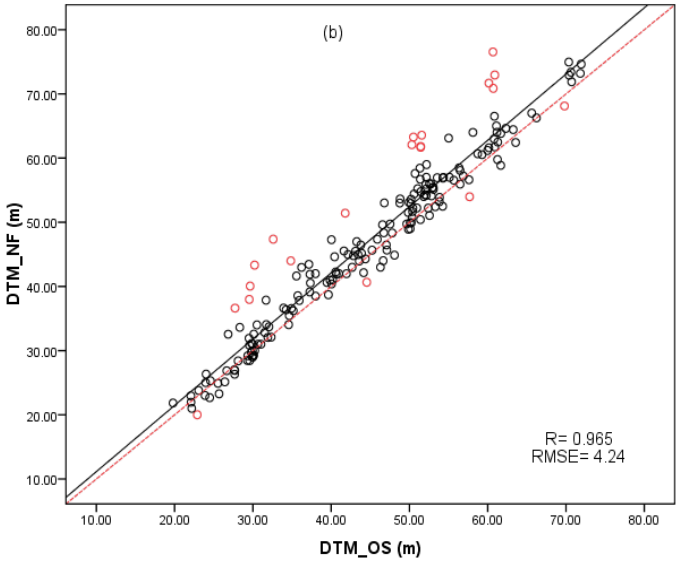
(b)
DTM_NF (m)
DTM_OS (m)
R= 0.965
RMSE= 4.24
10.00
20.00
30.00
40.00
50.00
60.00
70.00
80.00

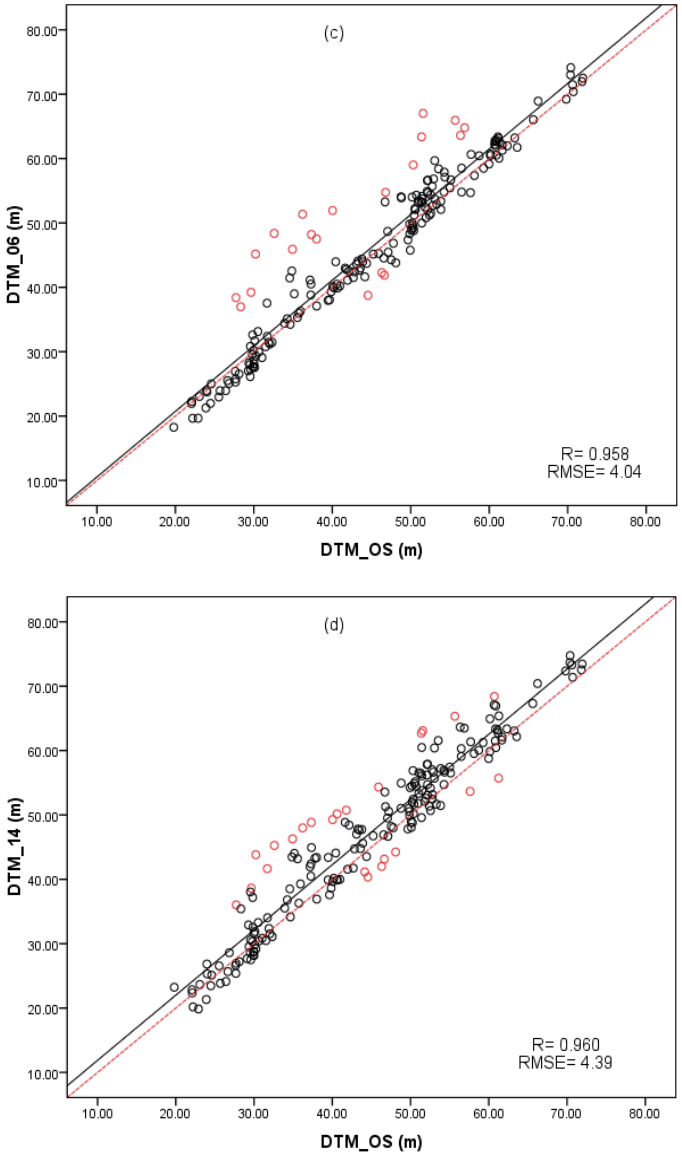

Figure 4.1: Relationship of (a) DTM_SRTM, (b) DTM_NF, (c) GLA06 and (d) GLA14 elevations with DTM_OS at Test Site A. Points in red indicate over and under estimated elevations. The red dotted line represents 1:1 line.

Figure 4.1 shows that DTM_OS is comparatively well correlated with DTM_SRTM (R=0.969) and DTM_NF (0.965) than with DTM_06 (0.958) and DTM_14 (0.960) for the given GLAS footprints. Because of coarser resolution of DTM_SRTM and DTM_NF, there is not much variation observed in Figure 4.1 (a) and (b), resulting in

higher correlation (Shafique et al., 2010). On the other hand, GLAS DTMs were interpolated at 2 m spatial resolution from point elevations. Apart from resolution, the lower coefficient of correlation of GLAS data can be attributed to linear but large scatter (in red). Similarly, the RMSE of DTM_14 is higher than the other three DTMs (DTM_SRTM, DTM_NF and DTM_06), which is because of the possible 'errors' it might have inherited during processing of GLA06 to get GLA14. 'Errors', here, refer to the uncertainties involved in ground peak detection using the correction flags in GLA06 and the associated method. It is important to mention that GLA06 elevations are obtained from the 'centroid' of the full-waveform (Brenner et al., 2003). On the contrary, GLA14 elevations are taken as the last peak of the waveform with maximum amplitude (Harding and Carabajal, 2005).

The lowest RMSE is depicted by DTM_06 which shows that the elevations predicted by GLA06 are more in agreement with DTM_OS (Figure 4.1 (c)). Additionally, DTM_06 elevations fall almost over the 1:1 line, showing the least bias compared to DTM_SRTM, DTM_NF and DTM_14. Contrary to DTM_06, DTM_14 has a higher upward bias but smaller scatter, resembling that of DTM_SRTM. These results show disagreement with Harding and Carabajal (2005), suggesting the waveform centroid as an indicator of ground height.

Moreover, a clear pattern can be noticed (red circles) in the correlation between GLAS data and DTM_OS (Figure 4.1 (c) & (d)). The pattern shows higher over-estimations than under-estimations, both in magnitude and number, unlike the findings of Duong et al. (2009). According to Duong et al. (2009), comparison of GLAS and airborne LASER elevations reported slight underestimation of terrain height by GLAS. To have an in-depth understanding of GLA06 and GLA14, spread of the residuals is shown in Figure 4.2.

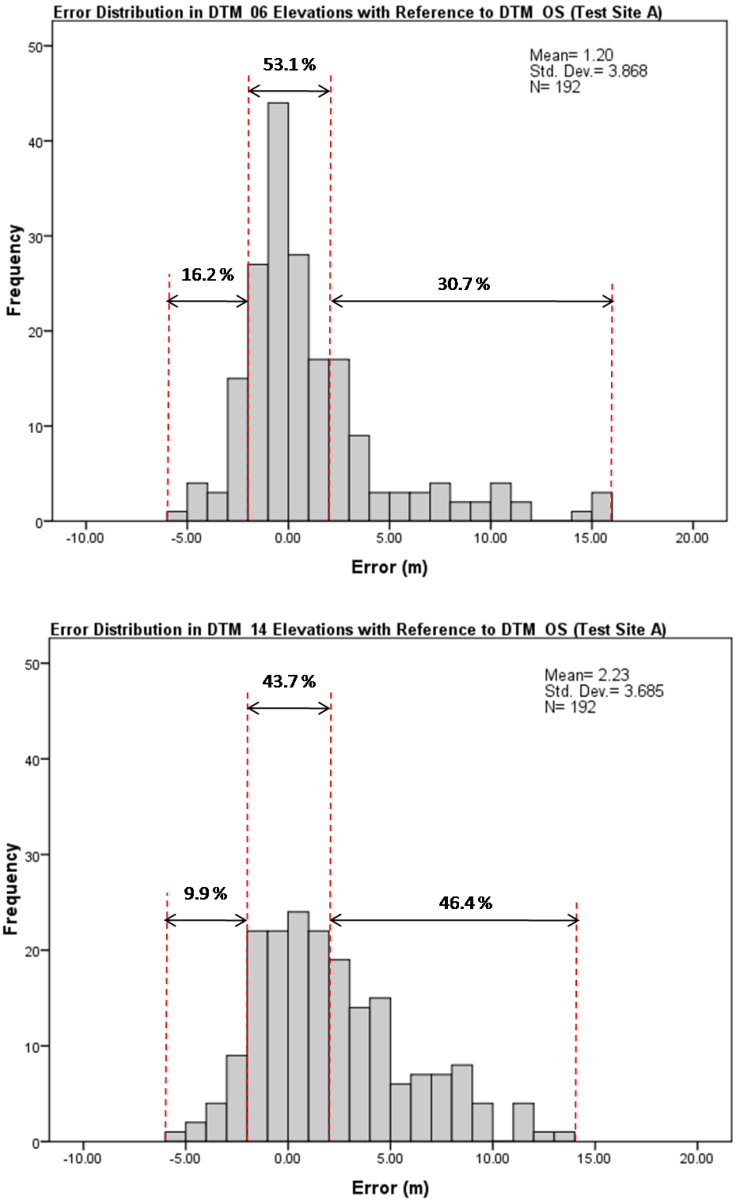

Figure 4.2: Comparative analysis of accurate, over and under estimated elevations obtained from GLA06 (top) and GLA14 (bottom) at Test Site A

In Test Site A, 53.1% of the GLA06 retrieved elevations accurately (±2 m) represented true ground, compared to the reference DTM. Nevertheless, 30.7% (>2 meters with a mean value of 6.6 m) was over-estimated and 16.2% (<2 m with a

mean value of -3.2 m) under-estimated. Similarly, 43.7% of the GLA14 predicted elevations accurately (±2 m) represented true ground; whereas, 46.4% (mean value of 6.1 m) of the predictions were over-estimated and 9.9% (mean value of -3.1 m) under-estimated. Furthermore, as shown in Figure 4.2, GLA14 has a slightly lower standard deviation (3.685) than GLA06 (3.868); however, when GLA14 is created using 'alternative parameterization', the percentage of accurately estimated elevations is compromised. This again indicates that the last peak with maximum amplitude is not the true representative of ground, as noted by Boudreau et al. (2008).

Results from similar analysis over Test Site B are presented in Figure 4.3, showing correlation of DTM_SRTM, DTM_06 and DTM_14 with DTM_OS. It should be noted that test site B did not have DTM_NF coverage and was not included in this analysis.

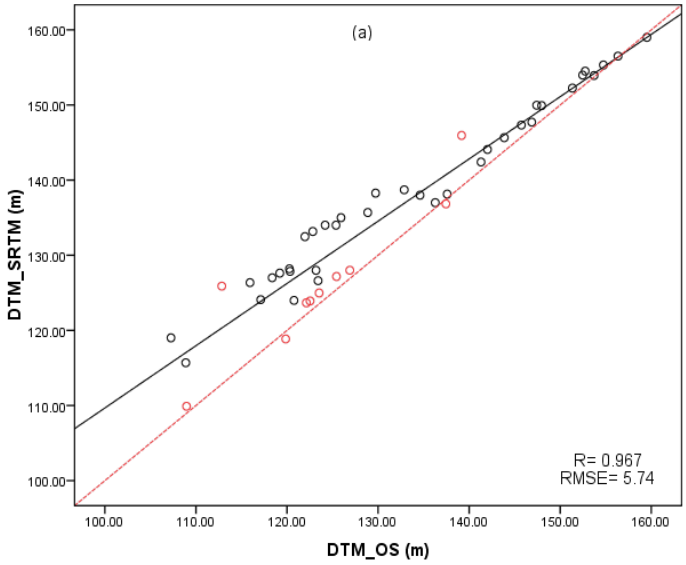
(a)
DTM_SRTM (m)
160.00
150.00
140.00
130.00
120.00
110.00
100.00
R= 0.967
RMSE= 5.74
100.00
110.00
120.00
130.00
140.00
150.00
160.00
DTM_OS (m)

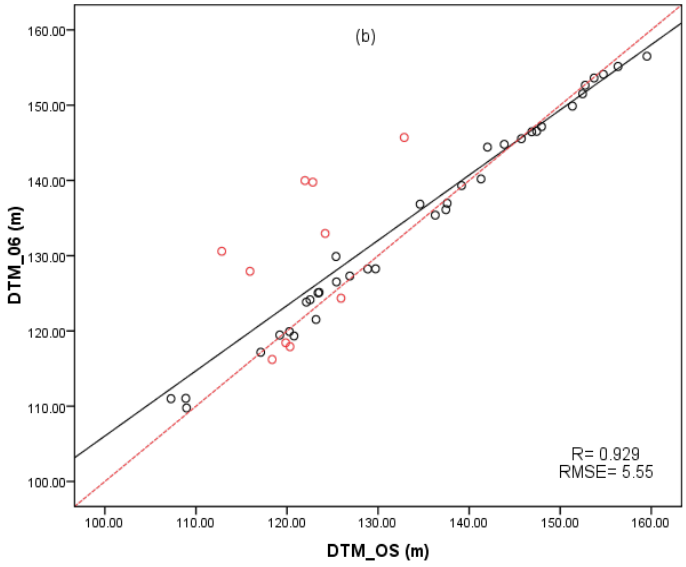
(b)
DTM_06 (m)
160.00
150.00
140.00
130.00
120.00
110.00
100.00
R= 0.929
RMSE= 5.55
100.00
110.00
120.00
130.00
140.00
150.00
160.00
DTM_OS (m)

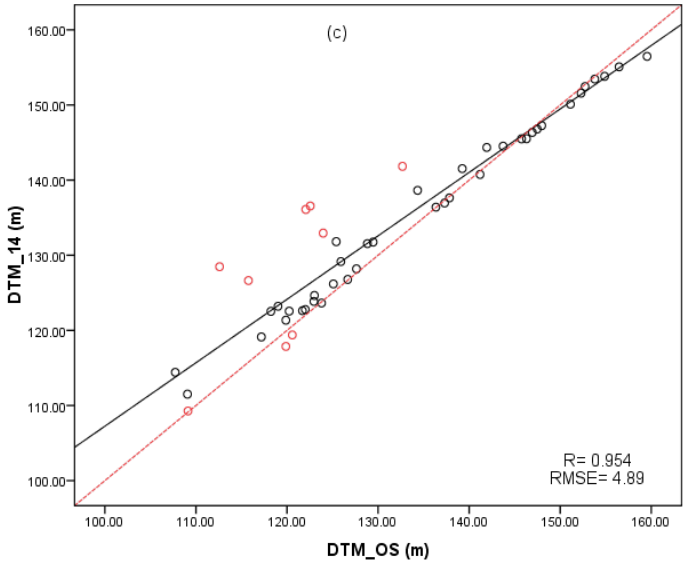

Figure 4.3: Relationship of (a) DTM_SRTM, (b) GLA06 and (c) GLA14 elevations with DTM_OS at Test Site B. Points in red indicate over and under estimated elevations. The red dotted line represents 1:1 line.

Figure 4.3 shows that GLAS data have lower coefficient of correlation (R-GLA06= 0.929 and R-GLA14=0.954) than DTM_SRTM (R-value=0.967); however, they have a slightly lower RMSE. Additionally, GLAS exhibits a lower intercept than that of DTM_SRTM, implying lower upward bias in elevations. However, GLAS highly exaggerates some of the elevations as shown in red circles in Figure 4.3 (b) and (c). Also, similar to test site A, the magnitude of over-estimation is significantly higher than that of under-estimation. On the other hand, DTM_SRTM elevations have a controlled spread, unlike GLAS data, showing more reliability in height prediction. However, GLAS predicted elevations cluster around 1:1 line, with few exceptions, showing more consistency with DTM_OS.

By comparing ground elevations predicted by GLA06 and GLA14, it seems that the two datasets almost follow the same pattern. At identical instances (red circles in Figure 4.3 (b) & (c)), the elevations are highly over-estimated, which correspond to thick vegetation cover with no or very little canopy gaps. Over test site B, GLA14 agrees with DTM_OS than GLA06 does, which indicates significance of considering the last peak as ground return. However, coefficient of correlation and RMSE alone are not explaining spread of the errors which is shown in Figure 4.4.

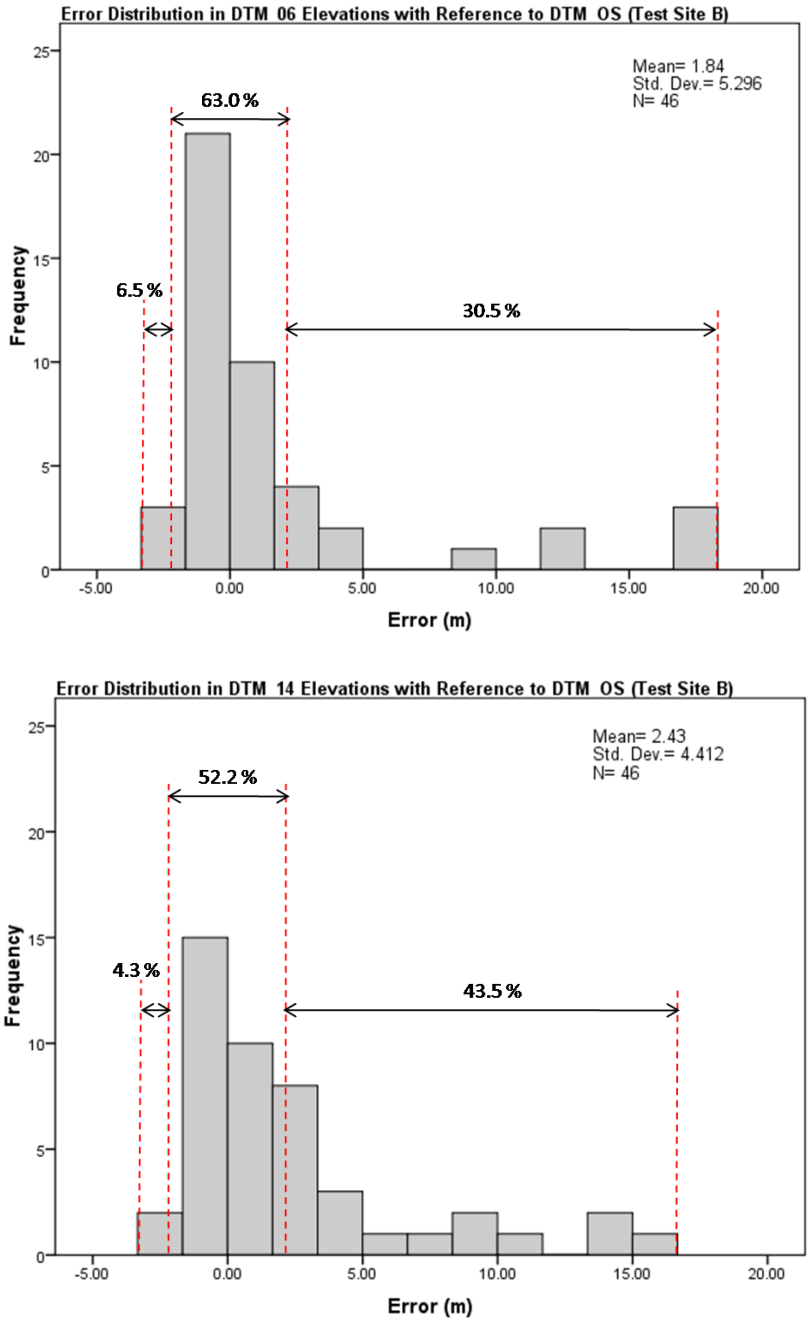

Figure 4.4: Comparative analysis of accurate, over and under estimated elevations obtained from GLA06 (top) and GLA14 (bottom) at Test Site B

Histograms in Figure 4.4 show that alongside improving the coefficient of correlation, RMSE and standard deviation, the processing has compromised the elevations which were accurately predicted in GLA06. On one hand, the under-estimated elevations have been accounted for while on the other hand the over-estimation has increased considerably. The pattern of shift in errors is similar to that at test site A.

4.1.1. Discussion

Investigations revealed that biases in GLAS derived DTMs occur over thick forest cover and/or where the canopy structure is coarser. However, in cases of sparse vegetation, deciduous trees with low canopy density, small built-up areas with clear surroundings and agricultural fields, GLAS elevations are consistent with DTM_OS (±2 m), because of minimal obstruction (Takeda, 2004).

Interestingly, irrespective of the forest type (conifer/broadleaved/mixed) in test site A and B, GLAS elevations are biased (either positively or negatively).

It can be inferred that high canopy density obstructs the LiDAR beam to penetrate and reach the ground. The energy which succeeds to reach the ground is weak and does not register a high intensity peak on reception. Alternatively, the peak with high amplitude is detected as ground and the remaining weak signal is binned closer to noise. If the trailing edge is assumed as ground, then it complies with the Ordnance Survey elevations. Figure 4.5 (a) & (b) shows two cases where GLAS derived surface elevations were over-estimated by 12.7 m and 7 m, respectively. In Figure 4.5 (a), the difference between 'GLAS ground' and 'DTM_OS ground', if calculated from the waveform is 9.2 m. Similarly, in Figure 4.5 (b), the difference is 6.15 m which are close to the over-estimation (12.7 m and 7 m, respectively) at these footprints. Trailing edge (in Figure 4.5 (a) and (b)) is possibly the response of litter scattered on forest floor which causes delay and decay of signal due to multiple scattering (Brenner et al., 2003, Mallet and Bretar, 2009). Over and under estimations due to litter depend on its thickness, three-dimensional distribution and spectral properties (Kimes et al., 2006). After multiple scattering, a strong signal will under-estimate the ground; whereas, weaker signal after multiple scattering will cause over-estimation due to increased path length (Brenner et al., 2003).

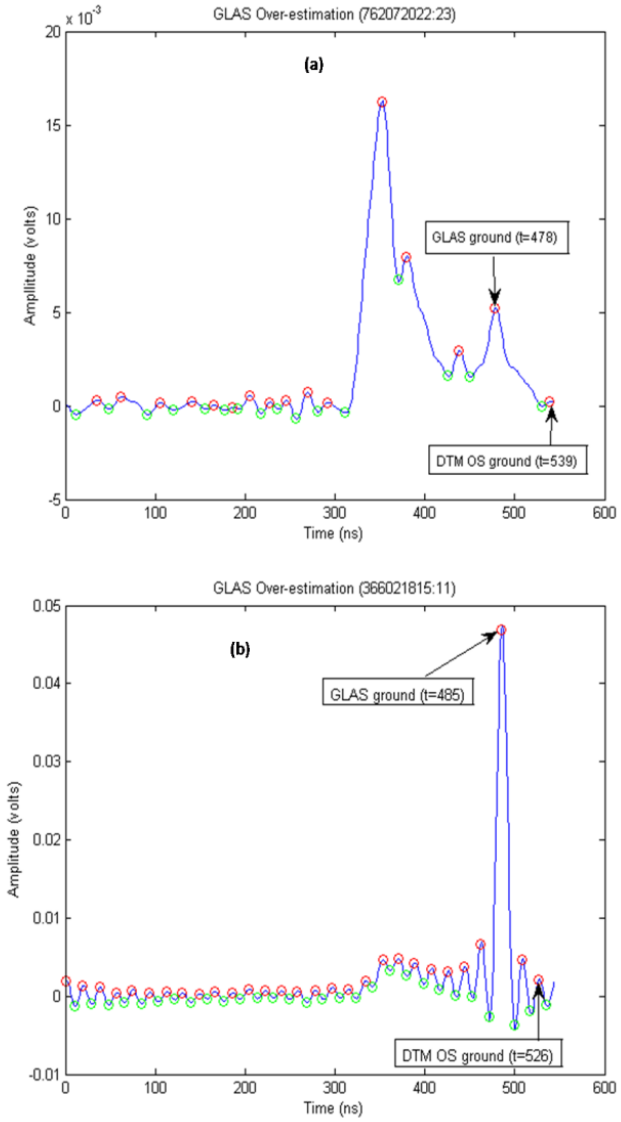

*Figure 4.5: Processed waveforms of surfaces which are 12.7 m (a) and 7 m (b) over-estimated by GLAS, as compared to DTM_OS. In (a), the difference between DTM_OS and GLAS is 9.2 m ((539-478)*0.15). Similarly, the difference calculated from (b) is 6.15 m. Waveform peaks and troughs are shown in red and green, respectively.*

In the test sites, GLAS estimated ground elevations are on average 6.6 meters higher than true ground heights with extreme cases up to 20 meters. It can be argued that since DTM_OS is a result of interpolated contours at 10 meters interval, it is

possible to have high topographic variations between two contours. Although, this argument may hold true in case of differences up to few meters; however, in cases where the difference is higher, the argument may not resist. Possible reason behind high over and under-estimations is within-footprint heterogeneity which is averaged by GLAS.

Furthermore, soil moisture may also be a factor which causes decay in the return pulse by absorbing some of the incoming energy (Brenner et al., 2003).

Above discussion indicates that there are complexities involved in estimating absolute ground elevation from GLAS waveforms which will be reflected in canopy height estimation. An over-estimated ground will result in under-estimated canopy height and vice-versa. This was addressed by objective 2 (Section 4.2 underneath).

4.2. Accuracy of GLAS derived canopy heights

Canopy heights calculated from field and Forestry Commission data correlated with those obtained from GLAS waveforms showed a correlation of 0.59, with an RMSE of 5.18 meters (Figure 4.6). Heights derived from GLAS waveforms are hereinafter referred to as 'GLAS Estimated Height'. Individual comparison of field and Forestry Commission heights with those derived from GLAS data is given in APPENDIX-III.

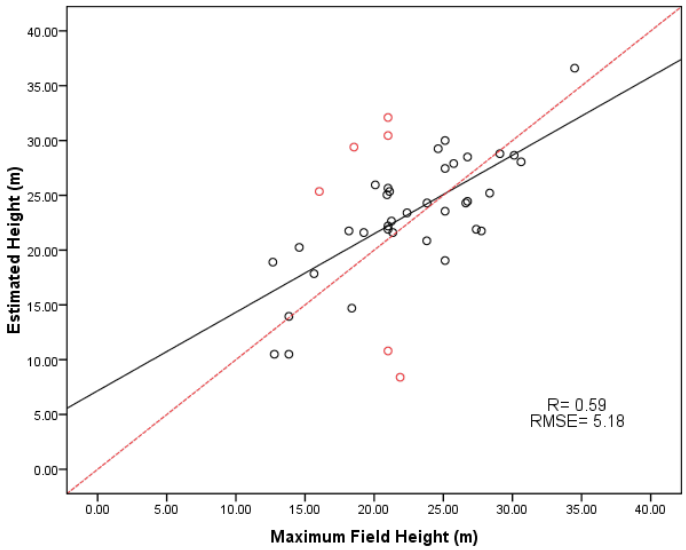

Figure 4.6: Correlation of canopy heights obtained from waveform analysis and those collected from field and Forestry Commission data. Outliers are shown in red. Red dotted line shows 1:1 line.

The offset of about six meters represents positive bias in GLAS estimated canopy heights. Also, the data has a wider spread around the correlation line. Low

correlation between the two datasets is because of few outliers, as shown in Figure 4.6 (in red). At these outliers, the over and under estimation of canopy heights were up to 11 and 13 meters, respectively. Analysis of these outliers revealed that over mixed and/or multiple canopies, the algorithm derived heights were positively biased. In cases of thick vegetation cover, the heights were under-estimated. Uncertainties in ground detection, as discussed in Section 4.1.1, further justify the bias in canopy heights.

4.2.1. Discussion

Waveforms of two extremely biased heights (11 m and -13 m) are presented in this section one after the other.

4.2.1.1. Extreme Over-estimation:

Figure 4.7 represents the waveform of a footprint which covered a sparse patch of oaks (196 years of age) dominated by low canopies. In the study area, oaks are not managed for commercial purposes; hence, height variations are expected. The LiDAR signal was excited by foliage of higher but few canopies, resulting in slight amplitude rise (red arrows in Figure 4.7); however, a strong response was registered from the lower canopies. For similar conditions, waveforms behaved the same way, resulting in over-estimated canopies. Vegetation structural heterogeneity is documented to complicate the relationship between LiDAR-derived and ground-derived canopy heights (Clark et al., 2004). Because the waveform behaviour was dictated by few trees, it was not a true representative of all vegetation within the footprint.

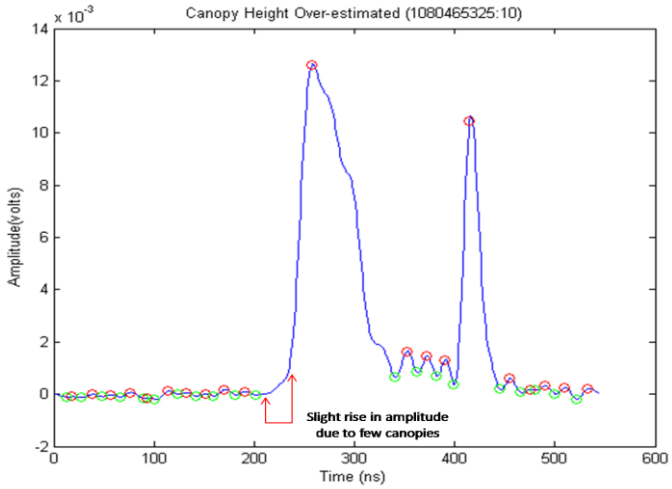

Figure 4.7: Extreme case of over-estimation up to 11 meters. Red and green circles show waveform peaks and troughs, respectively.

Figure 4.8 gives an aerial view of the location represented by waveform in Figure 4.7. The area is covered with old oaks, in which canopy heterogeneity can be noticed. The red circle represents the approximate footprint size.

Figure 4.8: Footprint location of waveform (in Figure 4.7). Red dot shows the footprint centre, labelled with record and shot number. Image taken from Google Earth (NOAA, 2009).

4.2.1.2. Extreme Under-estimation:

Figure 4.9 is a representative waveform where high under-estimation (13 m) in canopy height determination was observed. This footprint covered a young crop (29 years of age) of Douglas Fir with dense canopy, because of which the signal was obstructed. The signal, that penetrated the canopy, was weak and could hardly register a high amplitude peak. Another factor could be soil moisture, which is expected to be more under dense canopy cover, causing signal decay. Such conditions introduce uncertainties in precise ground detection, as discussed in Section 4.1.1., and ultimately result in biased canopy height estimates.

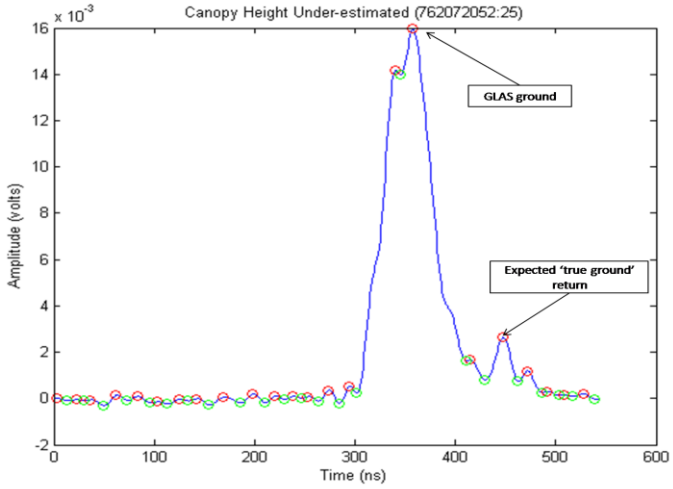

Figure 4.9: Extreme case of under-estimation up to 13 meters. Red and green circles show waveform peaks and troughs, respectively.

Figure 4.10 gives an aerial view of the location represented by waveform in Figure 4.9. The area is covered with young crop of Douglas Fir (29 years of age). The red circle approximates the footprint size.

Figure 4.10: Location of waveform (in Figure 4.9). The footprint, centred at red dot, covered young Douglas Fir crop. Image taken from Google Earth (NOAA, 2009).

Another important factor, to which GLAS data is reportedly sensitive, is crop age (Helmer and Lefsky, 2006, Sun and Ranson, 2000) which might have introduced bias in canopy heights estimated from waveforms. It should be noted that Figure 4.7 and 4.9 are representatives of footprints covered with old oaks (196 years) and young Douglas Fir (29 years), respectively.

It is interesting to note that four out of the six outliers fall within the Forestry Commission compartments, for which canopy heights were estimated from the Yield class curves. Only by removing these four outliers from analysis, the correlation improved from 0.59 to 0.72 and lowering RMSE from 5.18 m to 4.07 m, as shown in Figure 4.11.

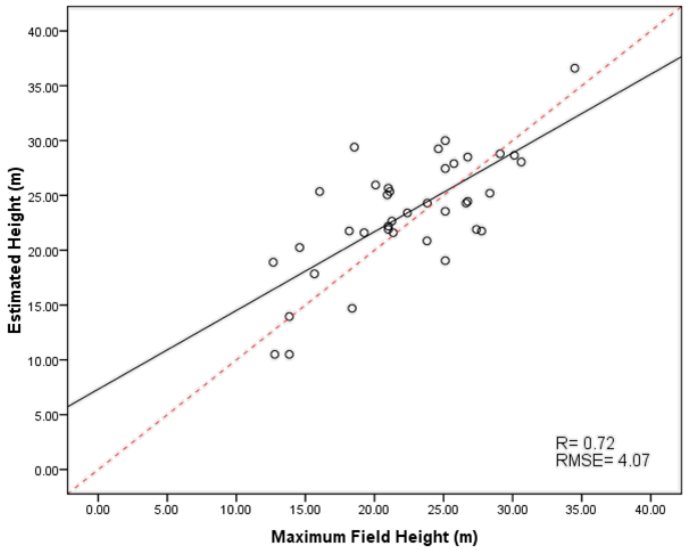

Figure 4.11: Improvement in R-value and RMSE, compared to Figure 4.6, after removal of four data points estimated from Yield class curves.

Figure 4.11 gives insights about the Yield class curves which were used to estimate canopy heights. Yield tables are species-specific generalized models created for compartments and sub-compartments, covering larger spatial extent than covered by GLAS footprint (about 70 m in diameter). There is a possibility that variation in site qualities exist on (sub) compartment level, which affects tree growth. Furthermore, Forestry Commission Yield models are not dynamic and depict a mean trend on (sub) compartment level (Rosette et al., 2008). This seems to be a valid reason for biases in canopy heights extracted from Yield class curves and those estimated with Fourier method. Moreover, this analysis demonstrates robustness of the new method of waveform processing for canopy height estimation, showing 'good' agreement with field measured heights.

Further, waveforms in Figure 4.7 and 4.9 are representatives of all the six outliers (Figure 4.6). Due to the uncertainties explained in Sections 4.2.1.1 and 4.2.1.2, these waveforms were removed to see the effectiveness of the Fourier method. Fourier heights obtained from the remaining waveforms showed an improved correlation with field measurements as shown in Figure 4.8.

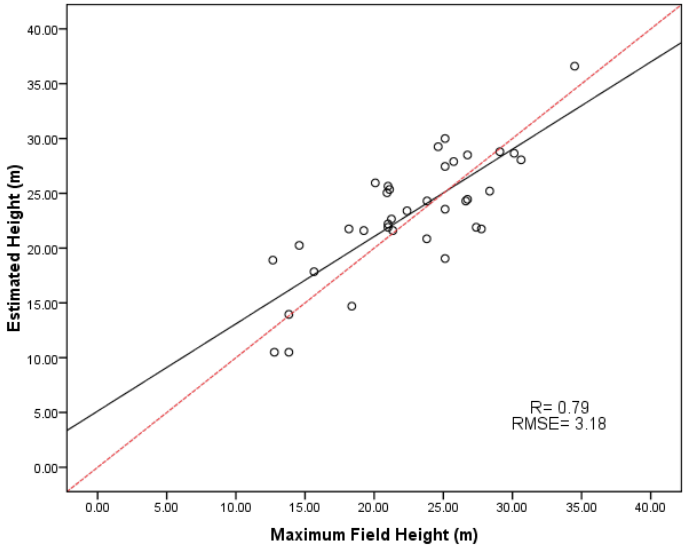

Figure 4.12: Correlation of field and GLAS estimated (Fourier) heights after removal of all six outliers.

Removal of six outliers (4 from Forestry Commission and 2 from field data) noticeably improved the coefficient of correlation from 0.59 to 0.79, and lowered the RMSE from 5.18 m to 3.18 m. With an automated method of ground identification based on iterative Gaussian fitting, Rosette et al. (2008) were able to explain 74 % of the variance in canopy heights in Forest of Dean, UK. It is logical to compare results from Rosette et al. (2008) with this study, because the two study sites (Forest of Dean and the New Forest National Park) have almost similar environmental conditions and are managed by Forestry Commission of Great Britain. It is important to mention that using DTM corrections, Rosette et al. (2008) were able to explain 89 % of variability in canopy heights. The method applied in this study, however, does not need topographic correction. This implies the advantage of Fourier method of waveform analysis to automatically estimate canopy heights in the absence of DTM.

4.3. Comparison of airborne and GLAS canopy heights

Canopy heights estimated from GLAS data and those from the airborne LiDAR were separately correlated with field measured heights as shown in Figure 4.13. Coefficient of correlation and RMSE were used as indicator of 'goodness of

agreement' between estimated and field-based measurements. Although the two areas were not spatially coincident, they had similar environmental and topographic conditions and were within the New Forest National Park.

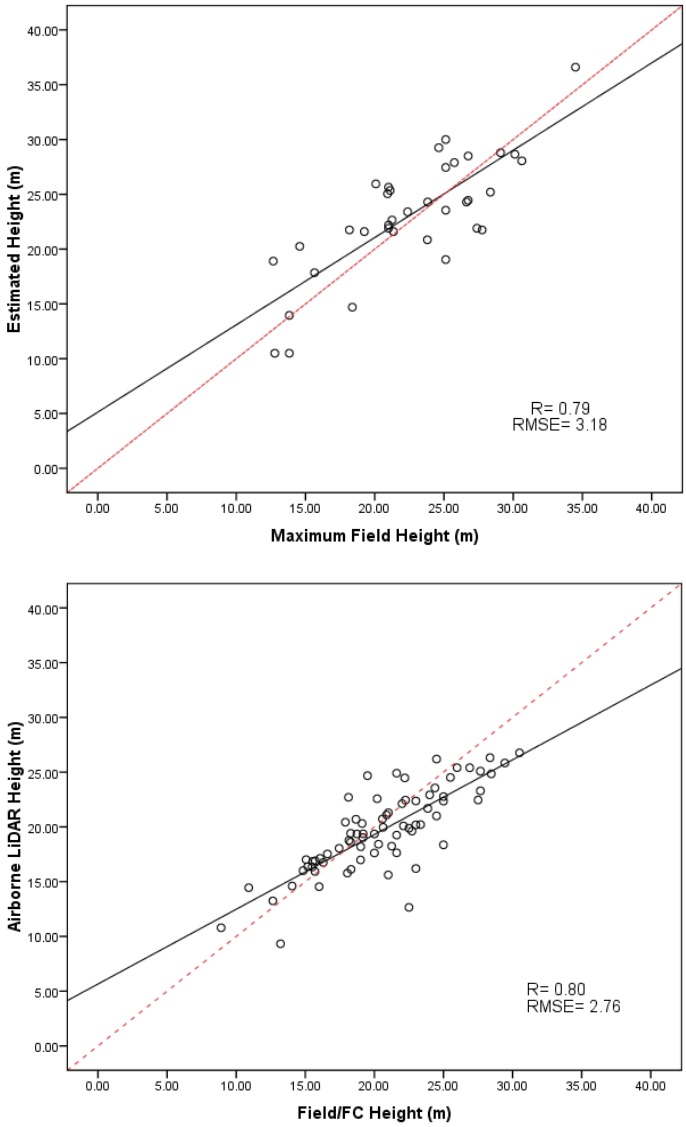

Figure 4.13: Comparison of performance of spaceborne/GLAS (top) and airborne (bottom) sensors under similar environmental and topographic conditions. Red dotted line indicates the 1:1 line.

From Figure 4.13, it is quite evident that airborne and GLAS height estimates are highly correlated with ground-based canopy heights with R-values of 0.80 and 0.79, respectively. GLAS estimated heights, however, have slightly higher RMSE (3.18 m) than airborne LiDAR (2.76 m).

Furthermore, GLAS estimated heights have a slightly lower intercept, showing a lower bias as compared to airborne data. Keeping in view the intricacies involved in GLAS estimated canopy heights from Section 4.2, the comparative lower bias might have been caused by its low sample number. It should also be noted that GLAS waveforms give maximum canopy height of the whole footprint. On the other hand, airborne LiDAR gives individual tree height because of high point density (1.2 points per m^2). This generalization of GLAS data has a smoothing effect on the overall bias, yielding lesser precision (Carabajal and Harding, 2001).

For the purpose of better visualization, GLAS and airborne heights are graphically compared with respective field measurements, as shown in Figure 4.14, and explained underneath.

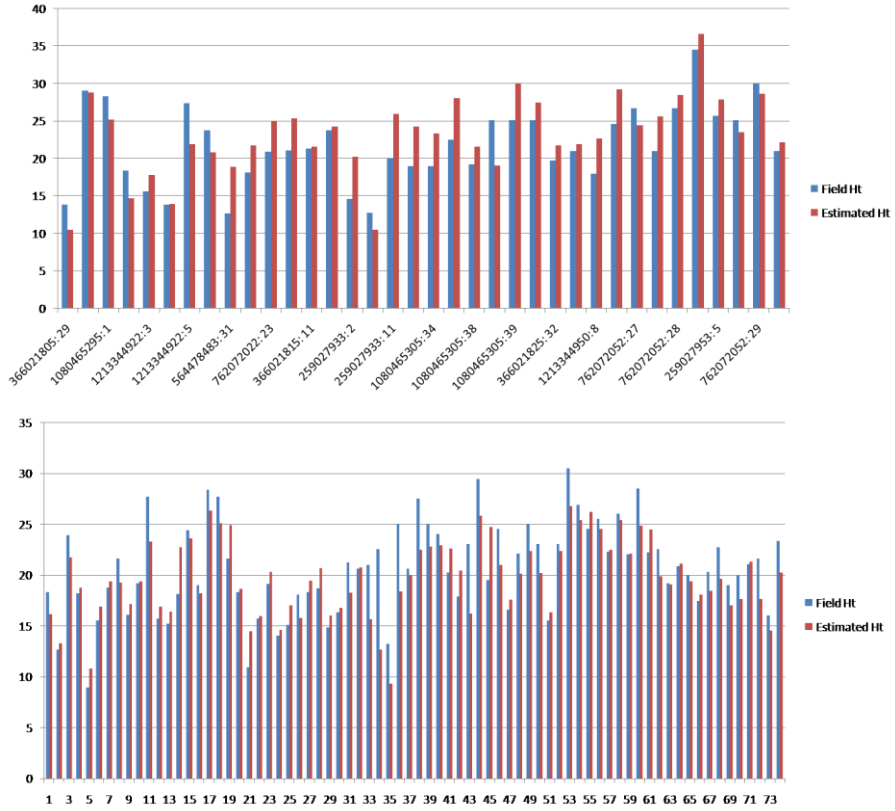

Figure 4.14: Graphical representation of field (blue) and estimated (maroon) heights measured from GLAS (top) and airborne (bottom) systems.

In Figure 4.14, field measured heights are represented by blue bars and GLAS/airborne estimated heights by maroon bars. The vertical axes (tree height) are in meters. Horizontal axes are labelled with point identities. Analysis of the two datasets revealed that 30.5% and 54% of canopy heights were under-estimated by GLAS and the airborne LiDAR, respectively.

4.3.1. Discussion

Results presented in Section 4.3 show that airborne LiDAR has under-estimated 54% of the canopy heights. There are two possible reasons for this under-estimation. Firstly, in discrete return systems the probability of hitting the canopy top is lower than hitting the 'tree shoulder' (Lefsky et al., 2002b, Dubayah et al., 1997). Secondly, limited pulse penetration to the ground through the canopy is reported to introduce errors in ground detection (Gaveau and Hill, 2003, Hyyppa et al., 2001). Approximately 25% of returns were considered as terrain points (Sumnall, 2009), which might have lowered the accuracy. However, with high point density (1.2 points per m^2) the airborne system was able to capture higher variability than GLAS.

Canopy heights estimated from GLAS data in the study area, had a general trend of over-estimation (69.5%) as compared to field measured heights. This exaggeration can be attributed to the uncertainties discussed in Sections 4.1 and 4.2. Nevertheless, the closer relationship between airborne and GLAS results shows the ability of the latter in global studies.

Other studies have also demonstrated good agreement between GLAS and airborne LiDARs; however no field data were used for validation. Duong et al. (2009), for example, reported a difference of 1.89 m between airborne LiDAR and GLAS height estimates over vegetated land cover. Similarly, Sun et al. (2008) were able to explain a maximum of 82% of variation in canopy height derived from LVIS.

Recently, indirect validation of GLAS derived biomass with field data was attempted, using airborne data as a link (Boudreau et al., 2008). A two-step approach was followed. First, Portable Airborne LiDAR system (PALS) was used for biomass estimation, resulting in an R^2 of 0.65 with field calculated biomass. Secondly, with the PALS results GLAS biomass estimates were evaluated. The agreement between PALS and GLAS was 0.54 (R^2). This result seems to be low due to dependency on PALS estimates, which are not true representation of the field measured biomass.

Specific studies on field-validation of airborne LiDAR and GLAS derived estimates are limited. Several studies, however, have shown good agreement of GLAS derived variables with field measurements.

In general, because of its high point density, airborne LiDAR has a higher spatial resolution than GLAS. This results in detailed and accurate information on vegetation structure, canopy height in this case. However, due to its discrete return and small footprint size, airborne LiDAR only records portions of the canopy. On

the other hand, full-waveform large-footprint LiDAR (such as GLAS) is capable of digitizing complete vertical structure of the canopy. In addition, full-waveform LiDARs offer information on canopy density which is represented by the amplitude strength.

Lastly, application of airborne and spaceborne LiDARs is more objective driven. Having global coverage, GLAS data can be used to extract regional and/global information. On the other hand, airborne LiDARs provide detailed local information. This marks a trade-off between the quality and spatial extent of information.

5. Conclusion and recommendation

5.1. Conclusion

Overall aim of the study was to evaluate the potential of ICESat/GLAS to estimate canopy height in the New Forest National Park, UK. Since GLAS derived height greatly depends on correct detection of ground return (Carabajal and Harding, 2001), it was of critical concern to analyse GLAS elevation products. Specific objectives of the study were to explore GLA06 and GLA14, estimate canopy height from GLA01 and compare the GLAS derived heights with an airborne LiDAR canopy height estimates. The study was successful to meet all the set objectives and answer the associated research questions.

To explore GLAS elevation products, two test sites were selected for this analysis. Test site A represented low land; whereas test site B had relatively higher elevation ranges. Raster surfaces (2 m resolution) created from GLA06 and GLA14 point elevations were individually compared with the reference surface (2 m resolution) created from Ordnance Survey maps. Additionally, SRTM (90 m) and an Interferometric Synthetic Aperture RADAR (IFSAR) (5 m) were also used to compare their performance with GLAS data. Despite different spatial resolutions, high correlation of all DTMs with DTM derived from Ordnance Survey data was indicative of low topographic variations and flat terrain in the study area. For this reason, slope factor was not included in analysis.

Two GLAS altimetry products (GLA06 and GLA14) were compared with the reference DTM to investigate their accuracy in estimating surface elevation. It was observed that thick and/or coarser canopies introduced bias in GLAS derived surface elevations. However, in areas where signal obstruction was minimal, GLAS elevations were consistent (±2 m) with DTM_OS. Possible reason for these biases is presence of litter on the forest floor, causing multiple scattering which attenuates the return pulse. Soil, in the study area, is most often damp due to the nature of forest type and weather conditions. Because GLAS operates in NIR (1064 nm) channel, pulse weakening due to soil moisture is also expected.

Individual analysis of GLA06 and GLA14 was also carried out which had interesting outputs. It was observed that at test site A, GLA06 had the lowest absolute error (RMSE=4.04 m) than the other DTMs. At test site B, however, GLA14 resulted in lower RMSE (4.89 m) than the other DTMs. Response of GLA06 and GLA14 to test sites A and B was logical. GLA06 is ‘designed’ for ice-sheet elevations where within footprint relief is not pronounced. GLA06 performed well at test site A because of its relatively flat terrain. GLA14, conversely, is derived for land altimetry accounting for surface properties such as relief variations. Test site B had

comparatively higher elevation ranges than test site A, which allowed GLA14 to perform well.

Further analysis of error distribution showed a positive shift in error from GLA06 to GLA14, at both sites. The frequency of over-estimation was higher in GLA14 as compared to GLA06. Although, the exact reason for this difference could not be investigated in this study; possible reason is the processing method by which GLA14 is obtained from GLA06. The unexplained variation may be due to GLAS positional errors (Duong et al., 2009, Carabajal and Harding, 2005).

Inaccuracies in ground peak detection have been reported to introduce uncertainties in canopy height estimation (Boudreau et al., 2008, Carabajal and Harding, 2005, Sun et al., 2008). This study demonstrated the ability of Fourier Transform to tackle such issues. Also, an automated method for detecting major peaks in the 'raw' waveform was developed. Due to signal attenuation, it was assumed that the actual ground return can be the peak with energy 20% lower than the peak of maximum amplitude. Effects of forest litter and soil moisture are possible reasons for signal weakening. With the methodology adopted, this study succeeded to explain 79% of the variation in canopy height estimation compared to field data. Justifications for the unexplained variance may be due to other factors like footprint eccentricity, representation of field measured height in GLAS data and energy decay between transmitted and received pulses, which were not investigated in this study.

Finally, results from airborne and spaceborne (GLAS) LiDARs were compared with field measured canopy height which showed high correlations. Although the two datasets were not spatially coincident, they represented similar environmental and topographic conditions and were within the New Forest National Park. GLAS and airborne LiDARs were able to explain 79% and 80% of variation in canopy height in the study area, respectively. GLAS estimated canopy heights, however, had a slightly higher RMSE (3.18 m) than airborne LiDAR (2.76 m). These results indicated the potential of GLAS in canopy height estimation over larger spatial extents.

5.2. Study limitations

a) Weather conditions and time limitation were the factors affecting the number of trees sampled in the field. It was attempted, however, to capture within-footprint canopy height variations.
b) Footprints used in terrain (DTM) and canopy height analysis were not the same. Should they be the same, this could have given supplementary insights on the biases in DTMs, reflected in canopy height using the so-called waveform-to-DEM matching analysis (Carabajal and Harding, 2001).
c) In this study, clinometer was used in the field for recording angles of elevation and depression of tree top and bottom, respectively. Tangent method was applied to workout canopy height. The tangent approach is

expected to introduce an error of about 1.1 m for an average maximum canopy height of 26.6 m (Rosette et al., 2008).

d) FC yield models are not dynamic and depict a mean trend on (sub) compartment level (Rosette et al., 2008). In this study, the highest deviations were observed between GLAS estimated and Yield model derived canopy heights. This suggested careful use of Yield curves for extracting height.

5.3. Recommendations

In future work, effect of footprint eccentricity, slope and energy decay between transmitted and receive pulse may be taken into account. Also, being beyond the scope of this study, the underlying processing method of GLA06 to get GLA14 was not investigated. Future work on this will expand understanding of the latent errors between the two products. The study succeeded to achieve encouraging results with minimum GLAS parameters. This implies that application of other ancillary variables and correction flags may enhance the results. Moreover, due to the possibility of losing some 'significant' peaks, the existing assumption of fitting six Gaussian modes to the raw waveform may be relaxed to include more Gaussian peaks.

There is a dearth of literature regarding comparison of airborne and spaceborne LiDAR estimates with field data. Studies on validation of spatially coincident airborne and spaceborne LiDARs data with field data are needed to evaluate these sensors.

Last but not the least, application of the presented methodology in other similar studies is strongly recommended to validate its repeatability and transferability.

References

Abshire, J. B., Sun, X., Riris, H., Sirota, J. M., McGarry, J. F., Palm, S., Yi, D. & Liiva, P. 2005. Geoscience Laser Altimeter System (GLAS) on the ICESat Mission: On-orbit measurement performance. *Geophys. Res. Lett.,* 32, L21S02. 10.1029/2005GL024028.

Ackermann, F. 1999. Airborne laser scanning--present status and future expectations. *ISPRS Journal of Photogrammetry and Remote Sensing,* 54**,** 64-67.

Aldred, A. H. & Bonnor, G. M. 1985. Application of airborne lasers to forest surveys. *Information Report PI-X-51, Canadian Forestry Service.* Petawawa National Forestry Institute

Andersen, H.-E., McGaughey, R. J. & Reutebuch, S. E. 2005. Estimating forest canopy fuel parameters using LIDAR data. *Remote Sensing of Environment,* 94**,** 441-449.

Blair, J. B., Rabine, D. L. & Hofton, M. A. 1999. The Laser Vegetation Imaging Sensor: a medium-altitude, digitisation-only, airborne laser altimeter for mapping vegetation and topography. *ISPRS Journal of Photogrammetry and Remote Sensing,* 54**,** 115-122.

Boudreau, J., Nelson, R. F., Margolis, H. A., Beaudoin, A., Guindon, L. & Kimes, D. S. 2008. Regional aboveground forest biomass using airborne and spaceborne LiDAR in Québec. *Remote Sensing of Environment,* 112**,** 3876-3890.

Brenner, A. C., Zwally, H. J., Bentley, C. R., Csathć, B. M., Harding, D. J., Hofton, M. A., Minster, J. B., Roberts, L., Saba, J. L., Thomas, R. H. & Yi, D. 2003. Derivation of Range and Range Distributions From Laser Pulse Waveform Analysis for Surface Elevations, Roughness, Slope, and Vegetation Heights. *Algorithm Theoretical Basis Document, Version 4.1.* Goddard Space Flight Center, Greenbelt, MD, USA. Unpublished. http://www.csr.utexas.edu/glas/atbd.html, 92 pp.

Carabajal, C. C., Boy, J.-P., Luthcke, S. B., Harding, D. J., Rowlands, D. D., Lemoine, F. G. & Chin, D. S. 2006. Recovery of Three-Gorges reservoir impoundment signal from ICESat altimetry and GRACE. *American Geophysical Union, Fall Meeting, abstract no. G13C-06,* 87 (52).

Carabajal, C. C. & Harding, D. J. 2001. Evaluation of Geoscience Laser Altimeter System (GLAS) waveforms for vegetated landscapes using airborne laser altimeter scanning data. *International Archives of Photogrammetry and Remote Sensing,* 34**,** 125:128.

Carabajal, C. C. & Harding, D. J. 2005. ICESat validation of SRTM C-band digital elevation models. *Geophys. Res. Lett.,* 32.

Carabajal, C. C. & Harding, D. J. 2006. SRTM C-band and ICESat laser altimetry elevation comparisons as a function of tree cover and relief. *Photogrammetric Engineering & Remote Sensing,* 72**,** 287-298.

Carson, W. W., Andersen, H.-E., Reutebuch, S. E. & McGaughey, R. J. Year. LiDAR applications in forestry-An overview. *In:* ASPRS, ed. ASPRS-70 years of service to the profession: Mountains of data-Peak decisions, May, 2004 Adams Mark Hotel. Denver, Colorado.

Clark, M. L., Clark, D. B. & Roberts, D. A. 2004. Small-footprint lidar estimation of sub-canopy elevation and tree height in a tropical rain forest landscape. *Remote Sensing of Environment,* 91**,** 68-89.

Dean, C., Roxburgh, S. & Mackey, B. G. 2004. Forecasting landscape-level carbon sequestration using gridded, spatially adjusted tree growth. *Forest Ecology and Management,* 194**,** 109-129.

Dobson, M. C., Ulaby, F. T., LeToan, T., Beaudoin, A., Kasischke, E. S. & Christensen, N. 1992. Dependence of radar backscatter on coniferous forest biomass. *Geoscience and Remote Sensing, IEEE Transactions on,* 30**,** 412-415.

Drake, J. B., Dubayah, R. O., Clark, D. B., Knox, R. G., Blair, J. B., Hofton, M. A., Chazdon, R. L., Weishampel, J. F. & Prince, S. 2002. Estimation of tropical forest structural characteristics using large-footprint lidar. *Remote Sensing of Environment,* 79**,** 305-319.

Dubayah, R., Blair, J. B., Bufton, J. L., Clark, D. B., JaJa, J., Knox, R., Luthcke, S. B., Prince, S. & Weishampel, J. Year. The Vegetation Canopy LiDAR Mission. *In:* Land Satellite Information in the Next Decade II: Sources and Applications, 1997. 100-112.

Dubayah, R., Knox, R., Hofton, M., Blair, J. B. & Drake, J. 2000. Land surface characterization using LiDAR remote sensing. *In:* HILL, M. J. & ASPINALL, R. J. (eds.) *Spatial Information for Land Use Management.* Singapore: Gordon and Breach Science Publishers.

Duong, H., Lindenbergh, R., Pfeifer, N. & Vosselman, G. 2007. ICESat full waveform altimetry compared to airborne laser altimetry over the Netherlands. *ISPRS Workshop on Laser Scanning 2007 and SilviLaser 2007.* Espoo, Finland.

Duong, H., Lindenbergh, R., Pfeifer, N. & Vosselman, G. 2009. ICESat Full-Waveform Altimetry Compared to Airborne Laser Scanning Altimetry Over The Netherlands. *IEEE Transactions on Geoscience and Remote Sensing,* 47**,** 3365-3378.

Duong, H., Pfeifer, N. & Lindenbergh, R. 2006a. Analysis of repeated ICESat full waveform data: methodology and leaf-on/leaf-off comparison. *Workshop on 3D Remote Sensing in Forestry.* Vienna.

Duong, H., Pfeifer, N. & Lindenbergh, R. 2006b. Full-waveform analysis: ICESat laser data for land cover classification. *Remote Sensing: From Pixels to Processes.* Enschede, the Netherlands: ISPRS Commission VII Mid-term Symposium.

Duong, V. H., Lindenbergh, R., Pfeifer, N. & Vosselman, G. 2008. Single and two epoch analysis of ICESat full waveform data over forested areas. *International Journal of Remote Sensing,* 29**,** 1453 - 1473.

EEA. 2009. *Corine land cover 2000 (CLC2000) 100 m - version 12/2009* [Online]. Available: http://www.eea.europa.eu/data-and-maps/data/corine-land-cover-2000-clc2000-100-m-version-12-2009 [Accessed October 5, 2009].

FCGB. 2009. *Forestry Commission in England* [Online]. Available: http://www.forestry.gov.uk/forestry/HCOU-5YHJS7 [Accessed September 22, 2009].

Gaveau, D. L. A. & Hill, R. A. 2003. Quantifying canopy height underestimation by laser pulse penetration in small-footprint airborne laser scanning data. *Canadian Journal of Remote Sensing,* 29**,** 650-657.

Geolas. 2007. *Application examples* [Online]. Available: http://www.geolas.com/Pages/indexE.html [Accessed June, 23 2009].

Gerck, E. & Hurtak, J. J. 1992. Laser remote sensing of forest and crop in genetic-rich tropical areas. *International Archives of Photogrammetry and Remote Sensing,* 29.

Gondal, M. A. & Mastromarino, J. 2000. Lidar system for remote environmental studies. *Talanta,* 53**,** 147-154.

Hamilton, G. J. & Christie, J. M. 1971. *Forestry Commission Booklet No. 34: Forest Management Tables (Metric)*, Her Majesty's Stationery Office, 1971.

Harding, D. J. & Carabajal, C. C. 2005. ICESat waveform measurements of within-footprint topographic relief and vegetation vertical structure. *Geophys. Res. Lett.,* 32.

Harding, D. J., Lefsky, M. A., Parker, G. G. & Blair, J. B. 2001. Laser altimeter canopy height profiles: methods and validation for closed-canopy, broadleaf forests. *Remote Sensing of Environment,* 76**,** 283-297.

Helmer, E. H. & Lefsky, M. A. 2006. Forest canopy heights in Amazon River Basin Forests as estimated with the Geoscience Laser Altimeter System (GLAS). *In:* AGUIRRE-BRAVO, C., PELLICANE, P. J., BURNS, D. P. & DRAGGAN, S. (eds.) *Monitoring Science and Technology Symposium: Unifying knowledge for Sustainability in the Western Hemisphere Proceedings RMRS-P-42CD.* Fort Collins, CO: U.S. Department of Agriculture, Forest Services, Rocky Mountain Research Station.

Hemery, G. E., Savill, P. S. & Pryor, S. N. 2005. Applications of the crown diameter-stem diameter relationship for different species of broadleaved trees. *Forest Ecology and Management,* 215**,** 285-294.

Hiratsuka, M., Toma, T., Ramada, M., Heriansyah, I. & Morikawa, Y. Year. A general allometric equation for estimating biomass in *Acacia mangium* plantations. *In:* Proceedings of the International Conference on Tropical Forests and Climate Change : carbon sequestration and clean development mechanism, October 21-22, 2003 Traders Hotel, Roxas Blvd. Manila: Conference Committee, xvii.

Houghton, R. A. 2005. Aboveground forest biomass and the global carbon balance. *Global Change Biology,* 11**,** 945-958.

Houghton, R. A. 2008. Biomass. *In:* SVEN ERIK, J. & BRIAN, F. (eds.) *Encyclopedia of Ecology.* Oxford: Academic Press.

Hubbard, W., Latt, C. & Long, A. 1998. *Forest terminology for multiple-use management* [Online]. University of Florida. Available: http://www.sfrc.ufl.edu/Extension/ssfor11.pdf [Accessed June 9 2009].

Hyyppa, H., Yu, X., Hyyppa, J., Kaartinen, H., Honkavaara, E. & Ronnholm, P. 2005. Factors affecting the quality of DTM generation in forested areas. *Proceedings of the ISPRS Workshop 'Workshop Laser Scanning 2005'.* Enschede, Netherlands: ISPRS.

Hyyppa, J. Year. Feasibility for estimation of single tree characteristics using laser scanner. *In:* IGARSS 2000. IEEE 2000 International Geoscience and Remote Sensing Symposium. Taking the Pulse of the Planet: The Role of Remote Sensing in Managing the Environment, 24-28 July 2000, 2000 Piscataway, NJ, USA. IEEE, 981-3.

Hyyppa, J., Hyyppa, H., Litkey, P., Yu, X., Haggren, H., Ronnholm, P., Pyysalo, U., Pitkanen, J. & Maltamo, M. 2004. Algorithms and methods of airborne laser scanning for forest measurements. *International Archives of Photogrammetry and Remote Sensing, Remote Sensing and Spatial Information Science,* 36 (Part 8/W2)**,** 82-88.

Hyyppa, J., Kelle, O., Lehikoinen, M. & Inkinen, M. 2001. A segmentation-based method to retrieve stem volume estimates from 3-D tree height models produced by laser scanners. *Geoscience and Remote Sensing, IEEE Transactions on,* 39**,** 969-975.

Hyyppae, J. M., Hyyppae, H. & Samberg, A. Year. Assessing forest stand attributes by laser scanner. *In:* KAMERMAN, G. W. & WERNER, C., eds., 1999 Orlando, FL, USA. SPIE, 57-69.

Ilvessalo, Y. 1950. On the correlation between the crown diameter and the stem of trees. *Publications of Finnish Forest Research Institute,* 38**,** 32.

IPCC. 2003. *Good Practice Guidance for Land Use, Land Use Change and Forestry* [Online]. Available: http://www.ipcc-nggip.iges.or.jp/public/gpglulucf/gpglulucf.html [Accessed August, 25 2009].

JNCC. 2006. *The New Forest SAC, Natura 2000 Standard Data Form* [Online]. Available: http://www.jncc.gov.uk/ProtectedSites/SACselection/n2kforms/UK0012557.pdf [Accessed June 9, 2009].

Junjie, Z. 2008. *Derivation of forest type information from large footprint spaceborne LIDAR waveforms : a case study in coll temperate forests of Northeastern China.* ITC.

Kato, A., Moskal, L. M., Schiess, P., Swanson, M. E., Calhoun, D. & Stuetzle, W. 2009. Capturing tree crown formation through implicit surface reconstruction using airborne lidar data. *Remote Sensing of Environment,* 113**,** 1148-1162.

Kaufman, Y. J., Tucker, C. J. & Fung, I. 1990. Remote sensing of biomass burning in the tropics. *Journal of Geophysical Research,* 95**,** 9927-9939.

Keller, M., Palace, M. & Hurtt, G. 2001. Biomass estimation in the Tapajos National Forest, Brazil: Examination of sampling and allometric uncertainties. *Forest Ecology and Management,* 154**,** 371-382.

Kilpatrick, D. J. & Savill, P. S. 1981. Top height growth curves for Sitka Spruce in Northern Ireland. *Forestry,* 54**,** 31-39.

Kimes, D. S., Ranson, K. J., Sun, G. & Blair, J. B. 2006. Predicting lidar measured forest vertical structure from multi-angle spectral data. *Remote Sensing of Environment,* 100**,** 503-511.

Kraus, K. & Pfeifer, N. 1998. Determination of terrain models in wooded areas with airborne laser scanner data. *ISPRS Journal of Photogrammetry and Remote Sensing,* 53**,** 193-203.

Kurtz, N. T., Markus, T., Cavalieri, D. J., Krabill, W., Sonntag, J. G. & Miller, J. 2008. Comparison of ICESat Data With Airborne Laser Altimeter Measurements Over Arctic Sea Ice. *Geoscience and Remote Sensing, IEEE Transactions on,* 46**,** 1913-1924.

Kwak, D. A., Lee, W. K. & Son, M. H. 2005. Application of LiDAR and digital aerial photography for precise forest inventory. *Proceedings of 2005 ESRI Internation User Conference.* San Diego, CA, U.S.A.: ESRI.

Kwok, R., Cunningham, G. F., Zwally, H. J. & Yi, D. 2006. ICESat over Arctic sea ice: Interpretation of altimetric and reflectivity profiles. *J. Geophys. Res.,* 111.

Leckie, D., Gougeon, F., Hill, D., Quinn, R., Armstrong, L. & Shreenan, R. 2003. Combined high-density lidar and multispectral imagery for individual tree crown analysis. *Canadian Journal of Remote Sensing,* 29**,** 633-649.

Lee, A. C. & Lucas, R. M. 2007. A LiDAR-derived canopy density model for tree stem and crown mapping in Australian forests. *Remote Sensing of Environment,* 111**,** 493-518.

Lefsky, M. A., Cohen, W. B., Harding, D. J., Parker, G. G., Acker, S. A. & Gower, S. T. 2002a. LiDAR remote sensing of above-ground biomass in three biomes. *Global Ecology & Biogeography,* 11**,** 393-399.

Lefsky, M. A., Cohen, W. B., Parker, G. G. & Harding, D. J. 2002b. LiDAR remote sensing for ecosystem studies. *BioScience,* 52**,** 19-30.

Lefsky, M. A., Harding, D., Cohen, W. B., Parker, G. & Shugart, H. H. 1999. Surface Lidar Remote Sensing of Basal Area and Biomass in Deciduous Forests of Eastern Maryland, USA. *Remote Sensing of Environment,* 67**,** 83-98.

Lefsky, M. A., Harding, D. J., Keller, M., Cohen, W. B., Carabajal, C. C., Del Bom Espirito-Santo, F., Hunter, M. O. & de Oliveira, R., Jr. 2005. Estimates of forest canopy height and aboveground biomass using ICESat. *Geophys. Res. Lett.,* 32, L22S02. doi:10.1029/2005GL023971.

Lefsky, M. A., Keller, M., Pang, Y., De Camargo, P. B. & Hunter, M. O. 2007. Revised method for forest canopy height estimation from Geoscience Laser Altimeter System waveforms. *Journal of Applied Remote Sensing,* 1.

Lim, K., Treitz, P., Wulder, M., St-Onge, B. & Flood, M. 2003. LiDAR remote sensing of forest structure. *Progress in Physical Geography,* 27**,** 88-106.

Lovell, J. L., Jupp, D. L. B., Newnham, G. J., Coops, N. C. & Culvenor, D. S. 2005. Simulation study for finding optimal lidar acquisition parameters for forest height retrieval. *Forest Ecology and Management,* 214**,** 398-412.

Lovell, L. J., Jupp, D. L. B., Culvenor, D. S. & Coops, N. C. 2003. Using airborne and ground-based ranging LiDAR to measure canopy structure in Australian forests. *Canadian Journal of Remote Sensing,* 29**,** 607-622.

Lucas, R. M., Lee, A. C. & Bunting, P. J. 2008. Retrieving forest biomass through integration of CASI and LiDAR data. *International Journal of Remote Sensing,* 29**,** 1553 - 1577.

Ma, R. 2005. DEM generation and building detection from LiDAR data. *Photogrammetric Engineering & Remote Sensing,* 71**,** 847-854.

Magnussen, S., Eggermont, P. & LaRiccia, V. N. 1999. Recovering Tree Heights from Airborne Laser Scanner Data. *Forest Science,* 45**,** 407-422.

Malhi, Y. & Grace, J. 2000. Tropical forests and atmospheric carbon dioxide. *Trends in Ecology & Evolution,* 15**,** 332-337.

Mallet, C. & Bretar, F. 2009. Full-waveform topographic lidar: State-of-the-art. *ISPRS Journal of Photogrammetry and Remote Sensing,* 64**,** 1-16.

Muukkonen, P. & Heiskanen, J. 2007. Biomass estimation over a large area based on standwise forest inventory data and ASTER and MODIS satellite data: A possibility to verify carbon inventories. *Remote Sensing of Environment,* 107**,** 617-624.

Næsset, E. 1997a. Determination of mean tree height of forest stands using airborne laser scanner data. *ISPRS Journal of Photogrammetry and Remote Sensing,* 52**,** 49-56.

Næsset, E. 1997b. Estimating timber volume of forest stands using airborne laser scanner data. *Remote Sensing of Environment,* 61**,** 246-253.

Næsset, E. & Bjerknes, K.-O. 2001. Estimating tree heights and number of stems in young forest stands using airborne laser scanner data. *Remote Sensing of Environment,* 78**,** 328-340.

NASA. 2003. *Ice, cloud, and land elevation satellite (ICESat)* [Online]. Available: http://icesat.gsfc.nasa.gov [Accessed June 11, 2009].

NASA. 2009a. *ICESat Home Page* [Online]. Available: http://icesat.gsfc.nasa.gov/ [Accessed January 23, 2009].

NASA. 2009b. *Shuttle Radar Topography Mission: the mission to map the world* [Online]. Available: http://www2.jpl.nasa.gov/srtm/ [Accessed October 5, 2009].

Nilsson, M. 1996. Estimation of tree heights and stand volume using an airborne lidar system. *Remote Sensing of Environment,* 56**,** 1-7.

NOAA. 2009. *Google Earth* [Online]. Available: http://earth.google.co.uk/ [Accessed August 31, 2009].

NSIDC. 2008. *GLAS Altimetry Product Usage Guidance* [Online]. Available: http://nsidc.org/data/docs/daac/glas_altimetry/pdf/NSIDC_AltUserGuide_Rel29.pdf [Accessed September 28, 2009].

NSIDC. 2009a. *GLAS Altimetry Data Dictionary* [Online]. Available: http://nsidc.org/data/docs/daac/glas_altimetry/data_dictionary.html [Accessed September 29, 2009].

NSIDC. 2009b. *ICESat/GLAS data: Tools* [Online]. Available: http://nsidc.org/data/icesat/tools.html [Accessed August 12, 2009].

OSGB. 2009. *Ordnance Survey data products* [Online]. Available: http://www.ordnancesurvey.co.uk/oswebsite/products/ [Accessed October 2, 2009].

Pang, Y., Lefsky, M., Sun, G., Miller, M. E. & Li, Z. 2008. Temperate forest height estimation performance using ICESat GLAS data from different observation periods. *The International Archives of the Photogrammetry, Remote Sensing and Spatial Information Science,* 37**,** 777-782.

Parker, G. G., Lefsky, M. A. & Harding, D. J. 2001. Light transmittance in forest canopies determined using airborne laser altimetry and in-canopy quantum measurements. *Remote Sensing of Environment,* 76**,** 298-309.

Popescu, S. C., Wynne, R. H. & Nelson, R. F. 2002. Estimating plot-level tree heights with lidar: local filtering with a canopy-height based variable window size. *Computers and Electronics in Agriculture,* 37**,** 71-95.

Popescu, S. C., Wynne, R. H. & Scrivani, J. A. 2004. Fusion of Small-Footprint Lidar and Multispectral Data to Estimate Plot- Level Volume and Biomass in Deciduous and Pine Forests in Virginia, USA. *Forest Science,* 50**,** 551-565.

Ranson, K. J., Sun, G., Kovacs, K. & Kharuk, V. I. Year. Landcover attributes from ICESat GLAS data in Central Siberia. *In:* Geoscience and Remote Sensing Symposium, 2004. IGARSS '04. Proceedings. 2004 IEEE International, 2004. 753-756.

Riaño, D., Meier, E., Allgöwer, B., Chuvieco, E. & Ustin, S. L. 2003. Modeling airborne laser scanning data for the spatial generation of critical forest parameters in fire behavior modeling. *Remote Sensing of Environment,* 86**,** 177-186.

Rosette, J. A. B., North, P. R. J. & Suárez, J. C. 2008. Vegetation height estimates for a mixed temperate forest using satellite laser altimetry. *International Journal of Remote Sensing,* 29**,** 1475 - 1493.

Schutz, B. E. 2001. Laser altimetry and lidar from ICESat/GLAS. *International Geoscience and Remote Sensing Symposium,* 2001, Vol. 3**,** 1016-1019.

Schutz, B. E. 2002. *Laser footprint location (geolocation) and surface profiles: Algorithm Theoretical Basis Document (Version 3.0)* [Online]. Available: http://www.csr.utexas.edu/glas/pdf/atbd_geoloc_10_02.pdf [Accessed June 4, 2009].

Schutz, B. E., Zwally, H. J., Shuman, C. A., Hancock, D. & DiMarzio, J. P. 2005. Overview of the ICESat mission. *Geophys. Res. Lett.,* 32**,** L21S01.

Shafique, M., Meijde, M. v. d., Kerle, N. & Meer, F. v. d. 2010. Impact of DEM source and resolution on topographic seismic amplication. *Internal Journal of Applied Earth Observation and Geoinformation,* Submitted January 4, 2010**,** 32.

Sithole, G. & Vosselman, G. 2004. Experimental comparison of filter algorithms for bare-Earth extraction from airborne laser scanning point clouds. *ISPRS Journal of Photogrammetry and Remote Sensing,* 59**,** 85-101.

Slobbe, D. C., Lindenbergh, R. C. & Ditmar, P. 2008. Estimation of volume change rates of Greenland's ice sheet from ICESat data using overlapping footprints. *Remote Sensing of Environment,* 112**,** 4204-4213.

Spinhirne, J. D., Palm, S. P., Hlavka, D. L., Hart, W. D. & Welton, E. J. 2005. Global aerosol distribution from the GLAS polar orbiting LiDAR instrument. Available: http://ieeexplore.ieee.org/stamp/stamp.jsp?arnumber=01494140.

St-Onge, B., Treitz, P. & Wulder, M. A. 2003. Tree canopy height estimation with scanning LiDAR. *In:* WULDER, M. A. & FRANKLIN, S. E. (eds.) *Remote sensing of forest environments: Concepts and case studies.* Kluwer Academic Publishers.

Stone, C., Coops, N. & Culvenor, D. 2000. Conceptual Development of a Eucalypt Canopy Condition Index Using High Resolution Spatial and Spectral Remote Sensing Imagery. *Journal of Sustainable Forestry,* 11**,** 23 - 45.

Suárez, J. C., Ontiveros, C., Smith, S. & Snape, S. 2005. Use of airborne LiDAR and aerial photography in the estimation of individual tree heights in forestry. *Computers & Geosciences,* 31**,** 253-262.

Sumnall, M. 2009. *Forest characterisation using combination of LiDAR and hyperspectral data.* M.Sc., University of Southampton.

Sun, G. & Ranson, K. J. 2000. Modeling lidar returns from forest canopies. *Geoscience and Remote Sensing, IEEE Transactions on,* 38**,** 2617-2626.

Sun, G., Ranson, K. J., Kimes, D. S., Blair, J. B. & Kovacs, K. 2008. Forest vertical structure from GLAS: an evaluation using LVIS and SRTM data. *Remote Sensing of Environment,* 12**,** 107-117.

Takeda, H. 2004. Ground surface estimation in dense forest. *The International Archives of the Photogrammetry, Remote Sensing and Spatial Information Science,* 35**,** 1016-1023.

Todd, K. W., Csillag, F. & Atkinson, P. M. 2003. Three dimensional mapping of light tranmittance and foliage distribution using LiDAR. *Canadian Journal of Remote Sensing,* 29**,** 544-555.

UNFCCC. 1997. *Kyoto Protocol to the United Nations Framework Convention on Climate Change* [Online]. Available: http://unfccc.int/resource/docs/convkp/kpeng.pdf [Accessed August 24, 2009].

UNFCCC. 2009a. *Copenhagen Accord* [Online]. Available: http://unfccc.int/files/meetings/cop_15/application/pdf/cop15_cph_auv.pdf [Accessed January 8, 2010].

UNFCCC. 2009b. *Fact sheet: Reducing emissions from deforestation in developing countries: approaches to stimulate action* [Online]. Available: http://unfccc.int/files/press/backgrounders/application/pdf/fact_sheet_reducing_emissions_from_deforestation.pdf [Accessed August 24, 2009].

URL1. 2009. *Edinburgh University Data Library* [Online]. Available: http://edina.ac.uk/digimap/ [Accessed September 12, 2009].

URL2. 2009. *United States Geological Survey* [Online]. Available: http://glovis.usgs.gov/ [Accessed August 14, 2009].

URL3. 2009. *Airborne Research and Survey Facility* [Online]. Available: http://arsf-dan.nerc.ac.uk/trac/wiki/Processing [Accessed August 20, 2009].

URL4. 2009. *ICESat/GLAS Data Subsetter* [Online]. Available: http://nsidc.org/forms/glas_subset_form.html [Accessed].

Wagner, W., Ullrich, A., Ducic, V., Melzer, T. & Studnicka, N. 2006. Gaussian decomposition and calibration of a novel small-footprint full-waveform digitising airborne laser scanner. *ISPRS Journal of Photogrammetry and Remote Sensing,* 60**,** 100-112.

Waring, R. H., Way, J., Hunt, E. R. J., Morrissey, L., Ranson, K. J., Weishampel, J. F., Oren, R. & Franklin, S. E. 1995. Imaging Radar for Ecosystem Studies. *BioScience,* 45**,** 715-723.

Wylie, D., Eloranta, E., Spinhirne, J. D. & Palm, S. P. 2007. A Comparison of Cloud Cover Statistics from the GLAS Lidar with HIRS. *Journal of Climate,* 20**,** 4968-4981.

Zadiraka, V. K. & Igisinov, K. 1973. Analysis of the accuracy and efficiency of the Fast Fourier Transform algorithm and some of its applications. *Cybernetics and Systems Analysis,* 9**,** 973-977.

Zwally, H. J., Schutz, B., Abdalati, W., Abshire, J., Bentley, C., Brenner, A., Bufton, J., Dezio, J., Hancock, D., Harding, D., Herring, T., Minster, B., Quinn, K., Palm, S., Spinhirne, J. & Thomas, R. 2002. ICESat's laser measurements of polar ice, atmosphere, ocean, and land. *Journal of Geodynamics,* 34**,** 405-445.

Zwally, H. J., Schutz, R., Bentley, C., Bufton, J., Herring, T., Minster, J., Spinhirne, J. & Thomas, R. 2006. GLAS/ICESat L1&L2 Global Land Surface Altimetry Data, Global Land Elevation Data V028/V029, 2003-2006. Boulder, CO: National Snow and Ice Data Center. GLAS/ICESat Data Subsetter.

Appendices

Appendix-I

Calibration tables in GLA01 header:

Calibration table 1 which is used by IDL programme to convert 'counts' to 'volts'. The count values ranges from 0-255. Each corresponding count has its own calibration value.

f_cnt2volttable[0,*] = $			
-0.195279	-0.188604	-0.181929	-0.175254
-0.168579	-0.161904	-0.155229	-0.148554
-0.141879	-0.135204	-0.128529	-0.121854
-0.115179	-0.108504	-0.101829	-0.095154
-0.088479	-0.081804	-0.075129	-0.068454
-0.061779	-0.055104	-0.048429	-0.041754
-0.035079	-0.028404	-0.021729	-0.015054
-0.008379	-0.001704	0.004971	0.011646
0.018321	0.024996	0.031671	0.038346
0.045021	0.051696	0.058371	0.065046
0.071721	0.078396	0.085071	0.091746
0.098421	0.105096	0.111771	0.118446
0.125121	0.131796	0.138471	0.145146
0.151821	0.158496	0.165171	0.171846
0.178521	0.185196	0.191871	0.198546
0.205221	0.211896	0.218571	0.225246
0.231921	0.238596	0.245271	0.251946
0.258621	0.265296	0.271971	0.278646
0.285321	0.291996	0.298671	0.305346
0.312021	0.318696	0.325371	0.332046
0.338721	0.345396	0.352071	0.358746
0.365421	0.372096	0.378771	0.385446
0.392121	0.398796	0.405471	0.412146
0.418821	0.425496	0.432171	0.438846
0.445521	0.452196	0.458871	0.465546
0.472221	0.478896	0.485571	0.492246
0.498921	0.505596	0.512271	0.518946
0.525621	0.532296	0.538971	0.545646
0.552321	0.558996	0.565671	0.572346
0.579021	0.585696	0.592371	0.599046
0.605721	0.612396	0.619071	0.625746
0.632421	0.639096	0.645771	0.652446
0.658924	0.665122	0.67132	0.677518
0.683716	0.689914	0.696112	0.70231
0.708508	0.714706	0.720904	0.727102
0.7333	0.739498	0.745696	0.751894
0.758092	0.76429	0.770488	0.776686
0.782884	0.789082	0.79528	0.801478
0.807676	0.813874	0.820072	0.82627
0.832468	0.838666	0.844864	0.851062
0.85726	0.863458	0.869656	0.875854
0.882052	0.88825	0.894448	0.900646
0.906844	0.913042	0.91924	0.925438
0.931636	0.937834	0.944032	0.95023
0.956428	0.962626	0.968824	0.975022
0.98122	0.987418	0.993616	0.999814
1.006012	1.01221	1.018408	1.024606
1.030804	1.037002	1.0432	1.049398
1.055596	1.061794	1.067992	1.07419
1.080388	1.086586	1.092784	1.098982
1.10518	1.111378	1.117576	1.123774
1.129972	1.13617	1.142368	1.148566
1.154764	1.160962	1.16716	1.173358
1.179556	1.185754	1.191952	1.19815
1.204348	1.210546	1.216744	1.222942
1.22914	1.235338	1.241536	1.247734
1.253932	1.26013	1.266328	1.272526
1.278724	1.284922	1.29112	1.297318
1.303516	1.309714	1.315912	1.32211
1.328308	1.334506	1.340704	1.346902
1.3531	1.359298	1.365496	1.371694
1.377892	1.38409	1.390288	1.396486
1.402684	1.408882	1.41508	1.421278
1.427476	1.433674	1.439872	1.44607

Appendix-I, Contd. (Calibration table2: Count to volt)

f_cnt2volttable[1,*] = $							
-0.193828	-0.187203	-0.180578	-0.173953	0.653941	0.660069	0.666197	0.672325
-0.167328	-0.160703	-0.154078	-0.147453	0.678453	0.684581	0.690709	0.696837
-0.140828	-0.134203	-0.127578	-0.120953	0.702965	0.709093	0.715221	0.721349
-0.114328	-0.107703	-0.101078	-0.094453	0.727477	0.733605	0.739733	0.745861
-0.087828	-0.081203	-0.074578	-0.067953	0.751989	0.758117	0.764245	0.770373
-0.061328	-0.054703	-0.048078	-0.041453	0.776501	0.782629	0.788757	0.794885
-0.034828	-0.028203	-0.021578	-0.014953	0.801013	0.807141	0.813269	0.819397
-0.008328	-0.001703	0.004922	0.011547	0.825525	0.831653	0.837781	0.843909
0.018172	0.024797	0.031422	0.038047	0.850037	0.856165	0.862293	0.868421
0.044672	0.051297	0.057922	0.064547	0.874549	0.880677	0.886805	0.892933
0.071172	0.077797	0.084422	0.091047	0.899061	0.905189	0.911317	0.917445
0.097672	0.104297	0.110922	0.117547	0.923573	0.929701	0.935829	0.941957
0.124172	0.130797	0.137422	0.144047	0.948085	0.954213	0.960341	0.966469
0.150672	0.157297	0.163922	0.170547	0.972597	0.978725	0.984853	0.990981
0.177172	0.183797	0.190422	0.197047	0.997109	1.003237	1.009365	1.015493
0.203672	0.210297	0.216922	0.223547	1.021621	1.027749	1.033877	1.040005
0.230172	0.236797	0.243422	0.250047	1.046133	1.052261	1.058389	1.064517
0.256672	0.263297	0.269922	0.276547	1.070645	1.076773	1.082901	1.089029
0.283172	0.289797	0.296422	0.303047	1.095157	1.101285	1.107413	1.113541
0.309672	0.316297	0.322922	0.329547	1.119669	1.125797	1.131925	1.138053
0.336172	0.342797	0.349422	0.356047	1.144181	1.150309	1.156437	1.162565
0.362672	0.369297	0.375922	0.382547	1.168693	1.174821	1.180949	1.187077
0.389172	0.395797	0.402422	0.409047	1.193205	1.199333	1.205461	1.211589
0.415672	0.422297	0.428922	0.435547	1.217717	1.223845	1.229973	1.236101
0.442172	0.448797	0.455422	0.462047	1.242229	1.248357	1.254485	1.260613
0.468672	0.475297	0.481922	0.488547	1.266741	1.272869	1.278997	1.285125
0.495172	0.501797	0.508422	0.515047	1.291253	1.297381	1.303509	1.309637
0.521672	0.528297	0.534922	0.541547	1.315765	1.321893	1.328021	1.334149
0.548172	0.554797	0.561422	0.568047	1.340277	1.346405	1.352533	1.358661
0.574672	0.581297	0.587922	0.594547	1.364789	1.370917	1.377045	1.383173
0.601172	0.607797	0.614422	0.621047	1.389301	1.395429	1.401557	1.407685
0.627672	0.634297	0.640922	0.647547	1.413813	1.419941	1.426069	1.432197

Appendix-II

The following format was used for recording field data. Tangent method was applied to convert angles (elevation and depression) to tree height.

Point No.	Elev. (m)	No. of Trees (32 cm <)					Site Description
		C (cm)	D_1	Θ_1	Θ_2	Species	

Elev = Elevation of footprint recorded with GPS (m)
C = Circumference (girth) of samples tree (cm)
D_1 = Distance from sampled tree (m)
Θ_1 = Angle of elevation of tree top (degrees)
Θ_2 = Angle of depression of tree base (degrees)

Appendix-III

These graphs show that most of the over-estimations in tree heights were observed in footprints for which data was taken from Yield curves.

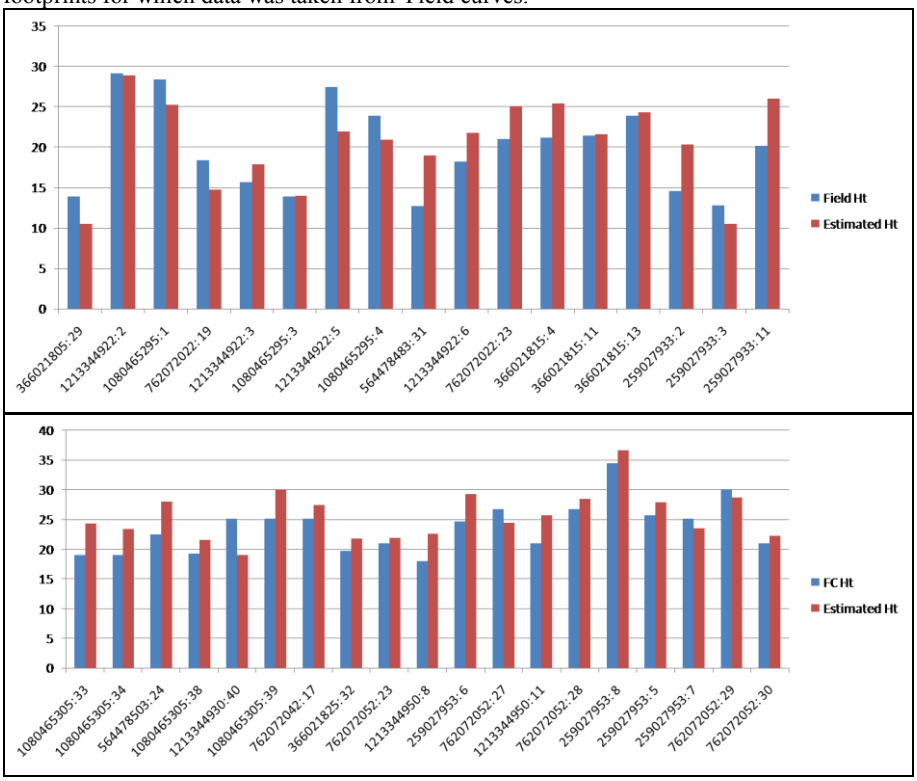

Top graph= GLAS height (maroon) and Field height (blue)
Bottom graph= GLAS height (maroon) and Forestry Commission height (blue)
Vertical axis= height in meters, Horizontal axis= point ID